International Journal of Biological Macromolecules 226 (2023) 628–645

Contents lists available at ScienceDirect

International Journal of Biological Macromolecules

journal homepage: www.elsevier.com/locate/ijbiomac

Divalent metal ion removal from simulated water using sustainable starch aerogels: Effect of crosslinking agent concentration and sorption conditions

Paulo H. Camani [a], C.D. Midhun Dominic [b], Duclerc F. Parra [c], Heloísa F. Maltez [d], Derval S. Rosa [a,*]

[a] Center for Engineering, Modeling, and Applied Social Sciences - CECS, Federal University of ABC (UFABC), Santo André, São Paulo 09210-580, Brazil
[b] Department of Chemistry, Sacred Heart College (Autonomous), Kochi, Kerala Pin-682013, India
[c] Institute of Research and Nuclear Energy - IPEN, São Paulo University (USP), Butantã, São Paulo 05508-000, Brazil
[d] Center for Natural and Human Sciences – CCNH, Federal University of ABC (UFABC) – Santo André, São Paulo 09210-580, Brazil

ARTICLE INFO

Keywords:
Corn starch
Aerogel
Potentially toxic elements

ABSTRACT

This paper evaluates corn starch aerogels, studying different crosslinking agent (trisodium citrate) concentrations (1:1, 1:1.5, and 1:2) and sorption conditions (contact time, adsorbent weight, and initial concentration) regarding the potentially toxic elements (PTEs) [Cd(II) or Zn(II)] adsorption of the aqueous systems. Besides, other properties of aerogels, such as structural properties, specific surface area, and mechanical performance, were evaluated. For adsorption results, better values were observed in adsorption capacity and efficiency for the initial concentration of 100 ppm. In addition, an adsorption time of 12 h and an adsorbent weight of 3.0 g obtained better results due to the possible balance in this time and the high specific surface area available for Cd (II) adsorption. As for the type of adsorbent, the Aero 1:1.5 sample (intermediate crosslinking agent concentration) obtained better results, possibly due to the high porosity, smaller pore sizes, high pore density, and high specific surface area (198 $m^2 \cdot g^{-1}$). In addition, hydroxyl groups in the starch aerogel removed Cd(II) ions with 30 % adsorption efficiency. Lastly, Aero 1:1.5 obtained a high mechanical strength at compression and a satisfactory compressive modulus. In contrast, starch aerogels did not absorb the Zn(II) ion.

1. Introduction

Water contamination is one of the causes of the degradation of water resources, with studies indicating their possible exhaustion in up to three decades [1,2]. These contaminants of water resources can be found in domestic effluents, industrial waste, surface, and groundwater [3,4]. Among these contaminants, one of the most worrying nowadays is *potentially toxic elements* (*PTEs*) due to their high mobility and bio-accumulation in living beings and humans, generating several problems [5,6].

Ion toxicity depends on mobility, influenced by the original mineral form, mobilization processes, and oxidation state [7,8]. Cadmium ion [Cd(II)] is a potentially toxic element found in the earth's crust, widely used in mining, processing metallic materials, battery production, and cigarette production [9]. It is a non-essential metal for human health, generating liver dysfunction, pulmonary edema, testicular damage, osteomalacia, damage to the adrenal glands, hematopoietic system, and, more aggressively, cancer [10]. In contrast, zinc ion [Zn(II)] is an essential metal, being a crucial micronutrient for new classes of enzymes and indispensable for the function of more than 300 enzymes [11]. However, it causes the breakdown of the plasma membrane zinc transfer set in large quantities, thus triggering apoptosis and even allowing cell death [12].

The partial or total removal of contaminants from water treatments is necessary to improve pre-and post-consumer water quality [13]. Recently, emerging removal methods have been gaining ground in investigations [14,15]. Adsorption has been gaining ground as a process of separation, purification, and/or detoxification on an industrial scale, which conventional and non-conventional materials can achieve, such as porous solids [16–19].

Adsorbents are reactive substrates with a high surface area to interact with contaminants and molecules [20,21]. *Aerogels* are highly porous structures that have been used as non-conventional adsorbents to remove contaminants from water [22]. Due to their high surface area, lightness, and compositional versatility, aerogels are excellent candidates for promoting contaminant adsorption, promoting remediation of

* Corresponding author.
E-mail address: derval.rosa@ufabc.edu.br (D.S. Rosa).

https://doi.org/10.1016/j.ijbiomac.2022.11.308
Received 25 September 2022; Received in revised form 26 November 2022; Accepted 29 November 2022
Available online 2 December 2022

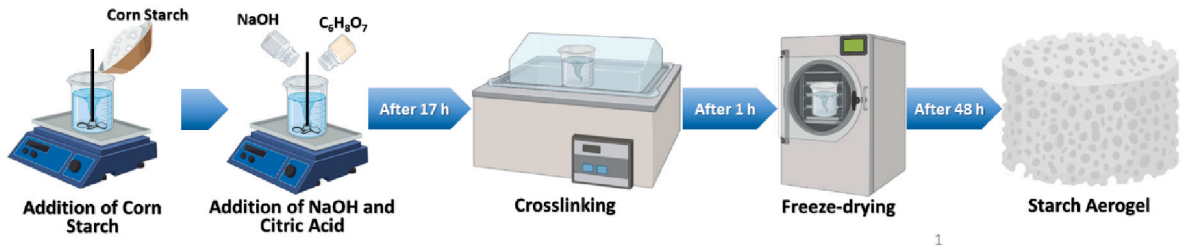

Fig. 1. Step-by-step scheme of starch-aerogel preparation.

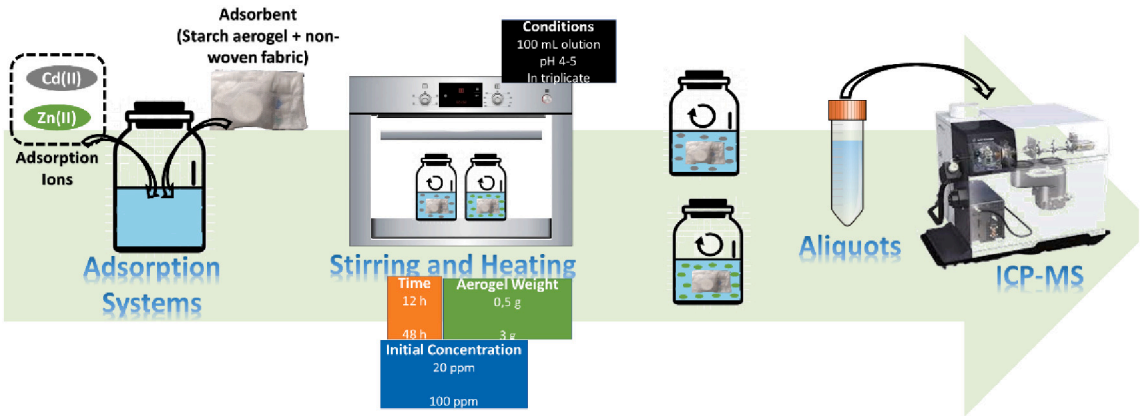

Fig. 2. Scheme of the steps related to the study of adsorption of corn starch aerogels by ICP-MS.

Fig. 3. The visual aspect of corn starch aerogels, highlighting Aero 1:1 (red circle), Aero 1:1.5 (blue circle, and Aero 1:2 (green circle), respectively.

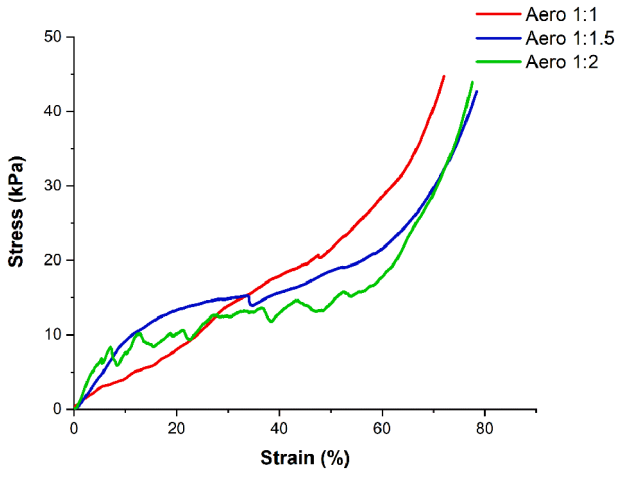

Fig. 4. Stress (kPa) versus strain (%) curves for corn starch aerogels.

contaminated areas [23–26]. One of the current materials used to prepare aerogels is polymers, in which polysaccharides are promising molecules to synthesize these porous structures [27,28].

In recent years, numerous papers have brought applications of functionalized materials, such as composite materials containing the chelating agent, to improve the PTEs' removal from contaminated water. However, most current functionalized adsorbent systems cover research for composite materials from silica and sensors containing organic molecules for the removal of metal ions, dyes, and organic compounds

Table 1
Mechanical performance values for corn starch aerogels.

Mechanical performance values	Starch aerogels		
	Aero 1:1	Aero 1:1.5	Aero 1:2
Compressive modulus (kPa)	107.4 ± 1.0	100.5 ± 0.7	123.0 ± 4.0
Maximum compressive strength (kPa)	37.5 ± 4.3	33.4 ± 0.7	31.0 ± 3.0
Maximum strain at compression (%)	68.0 ± 4.3	75.1 ± 3.0	73.3 ± 4.5
5 % strain strength (kPa)	3.5 ± 1.0	5.6 ± 1.2	10.0 ± 3.0
10 % strain strength (kPa)	7.0 ± 1.6	8.4 ± 1.0	8.0 ± 2.0
20 % strain strength (kPa)	11.2 ± 2.0	10.0 ± 1.3	11.3 ± 1.0

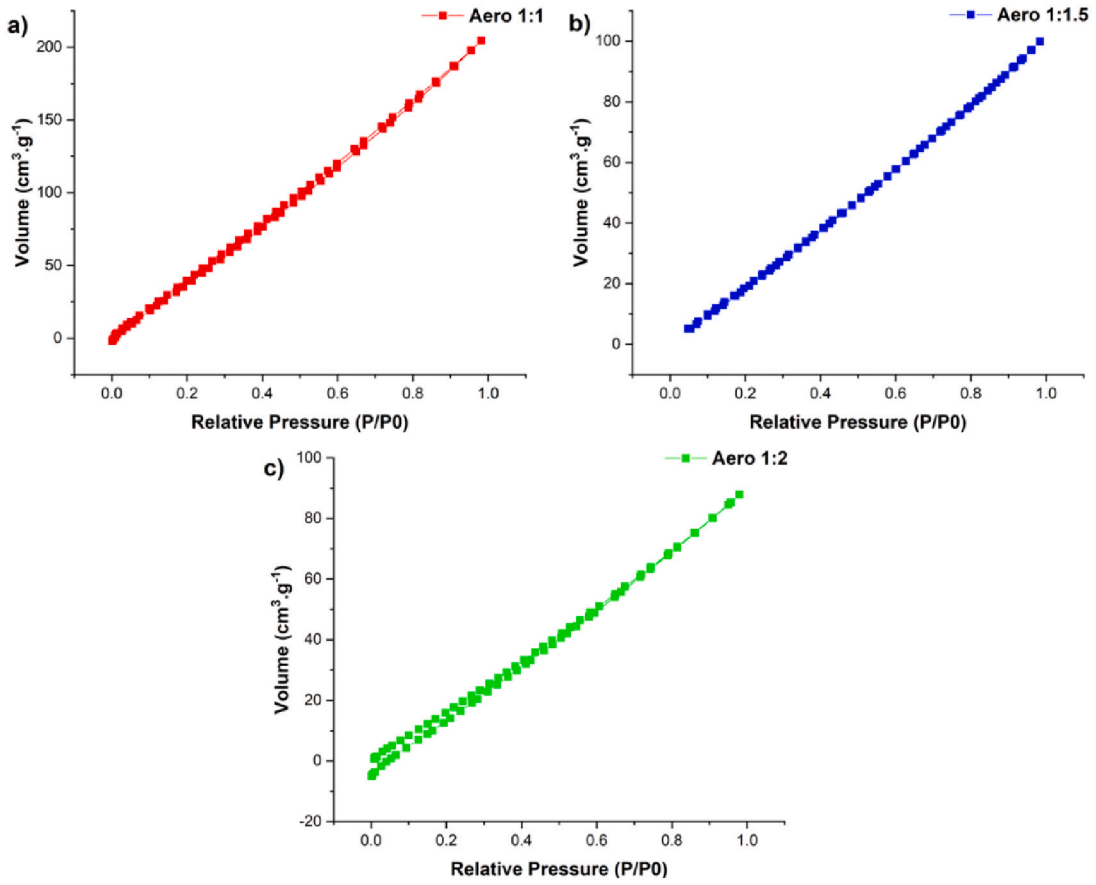

Fig. 5. Nitrogen adsorption/desorption isotherm curves by BET surface area analysis of corn starch aerogels prepared by varying the crosslinking agent concentration (Aero 1:1, Aero 1:1.5, and Aero 1:2).

Table 2
Average values of BET-specific surface area, pore diameter, and pore volume for corn starch aerogels.

Samples	Specific surface area ($m^2 \cdot g^{-1}$)	Pore diameter (nm)	Pore volume ($cm^3 \cdot g^{-1}$)
Aero 1:1	403.0	2.3	0.42
Aero 1:1.5	198.0	2.6	0.24
Aero 1:2	183.5	2.4	0.18

[29–44]. However, chelating agents such as aminopolycarboxylic acids (APCAs) and organic molecules may cause severe problems when functionalized materials containing these compounds are disposed on the environment. Studies point out that these compounds (such as nitrogenous and reactive molecules) cause eutrophication when discarded in ecosystems due to the increased proliferation of algae generated. It occurs by releasing nitrogen in the liquid medium. In addition, there is the possibility of promoting the destruction of cell membranes of some types of bacteria, promoting the impoverishment of the local soil or the quality of water bodies [45,46]. Thus, this paper investigated sustainable and biodegradable materials to develop a porous adsorbent to remove PTEs from contaminated water.

Starch is considered the second polysaccharide more abundant on the planet [47]. Due to its abundant presence of hydroxyl functional groups in starch structure and eco-friendly approach, this material is promising for developing sustainable adsorbents [48]. However, low works used starch aerogels to adsorb contaminants. Hammi et al. developed HKUST-1 and ZIF-8 in a colloidal solution of different molecular weight chitosan biopolymers. One of the colloidal solutions used

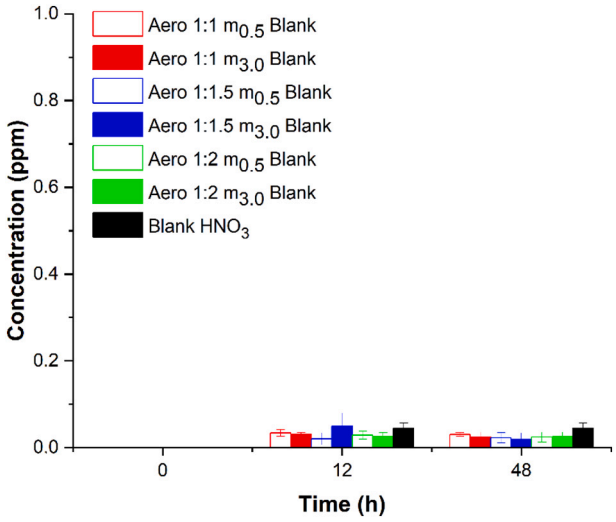

Fig. 6. Concentration (ppm) results after adsorption for the Blank systems and the acidic NaOH solution without the adsorbent related to Cd^{2+} systems.

was starch and chitosan as templating to remove Red congo dye from contaminated water [49]. However, in this work, starch was used to support removing the contaminant. Thus, this work aims to evaluate corn starch aerogels with different crosslinking agent concentrations (corn starch proportion: crosslinking agent) regarding the adsorption capacity and efficiency related to aqueous systems containing Cd(II) and Zn(II) ions alone, as well as their mechanical performance. Besides,

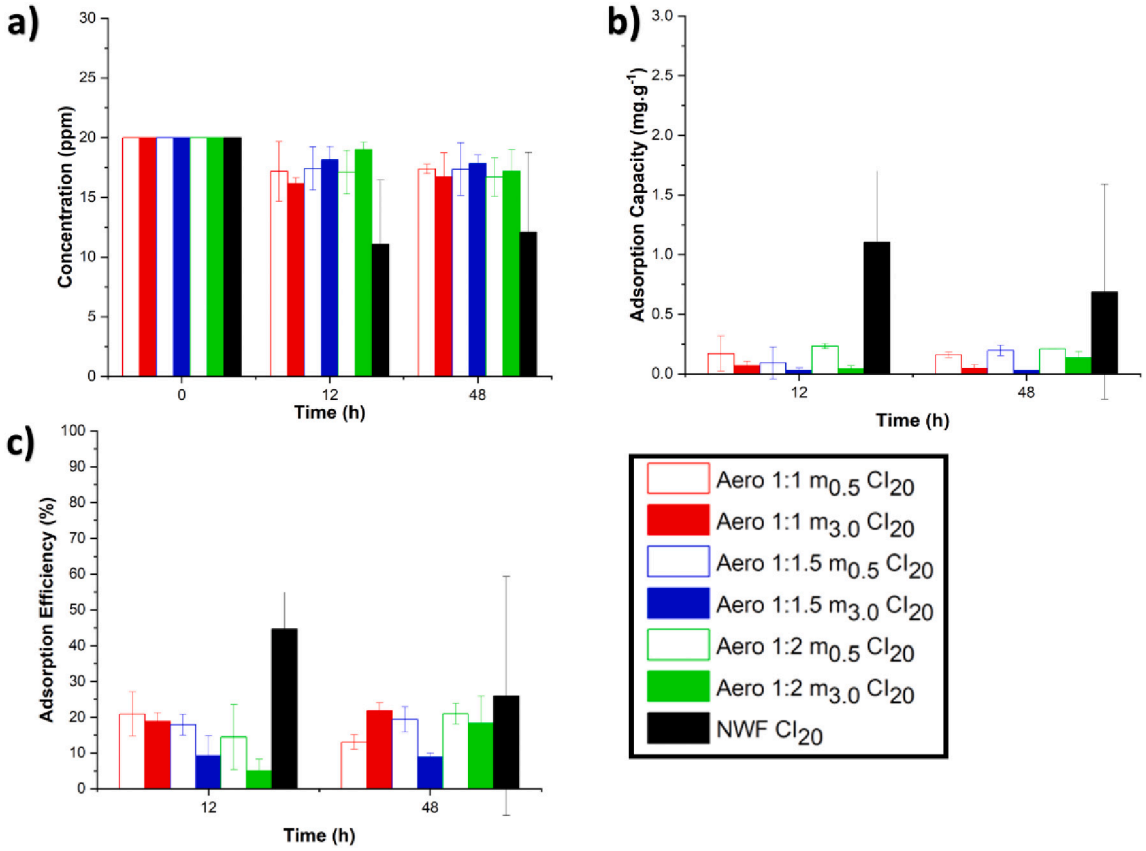

Fig. 7. Results of **a)** concentration (ppm) after adsorption, **b)** adsorption capacity ($mg{\cdot}g^{-1}$), and **c)** adsorption efficiency (%) for systems containing the divalent cadmium ion at an initial concentration of 20 ppm, varying the type of adsorbent and the weight, related to the measured times, respectively.

condition sorption, such as adsorbent weight, time, and initial concentration, was investigated to comprehensively in-depth the system sorption of these metal ions.

2. Experimental

2.1. Materials

The corn starch aerogels were developed from corn starch, containing 27 % (w/w) of amylose and 73 % (w/w) of amylopectin, which was supplied by Corn Products Brazil (PRODUCTS®/CASCO® Industrial Corn Starch - 030050). Sodium hydroxide was purchased from Casa Americana (São Paulo, Brazil), citric acid was purchased from Synth (São Paulo, Brazil), and distilled water was used to prepare all the aerogel solutions.

The study of the adsorption of divalent metal ions [Cd(II) and Zn(II)] by starch aerogels was carried out using metal ion salts in the form of nitrates [cadmium nitrate tetrahydrate PA (Exodo, São Paulo, Brazil) ($CdN_2O_6{\cdot}4H_2O$) and zinc nitrate hexahydrate PA (Dinamica, São Paulo, Brazil) ($Zn(NO_3)_2{\cdot}6H_2O$), distilled water, milli-Q water, sodium hydroxide PA (NaOH), nitric acid PA (HNO_3) (Synth, São Paulo, Brazil), and distilled nitric acid.

2.2. Aerogel synthesis

The corn starch aerogels were prepared from adaptations of the methodology described by Abhari, Madadlou, and Dini [50] and previously developed and published in a previous paper [47]. The preparation methodology was synthesizing a corn starch aerogel, crosslinked by citric acid in a base medium (formation of trisodium citrate) and dried by freeze-drying. The nomenclature of the samples was based on the proportion of corn starch and crosslinking agent, respectively (Aero 1:1, Aero 1:1.5, and Aero 1:2). Fig. 1 elucidates the step-by-step methodology used to prepare starch aerogels.

2.3. Characterizations

2.3.1. Visual aspect

The visual aspect of corn starch aerogels before and after adsorption tests were evaluated from images obtained by a Xiaomi Technology Co. Ltd. camera (Haidian District, Beijing, China), with a resolution of 8000 × 6000 pixels, digital light stabilization, and a sensor size of 1/two ″.

2.3.2. Shrinkage rate

The aerogel's shrinkage is an essential characteristic of the development of aerogels. This aspect depends on the drying type and the intrinsic structure of the material. The shrinkage rate (%) is given by the variation in dimensions of the hydrogel and aerogel after drying, as described by Wang et al. Eq. (1) describes the diameter variation of the hydrogel (L_0) and the aerogel (L_f) formed after drying by lyophilization [51]. The measurements of the diameter of the aerogels were performed in quadruplicates, with the aid of a digital caliper, measuring them in millimeters (mm).

$$\text{Shrinkage Rate}\ (\%) = \frac{L_0 - L_f}{L_0} \times 100\% \quad (1)$$

2.3.3. Mechanical compressive analysis

Mechanical compressive analysis was performed to evaluate compressive modulus (kPa), compressive strength (kPa), and strain at break (%). This analysis was adapted from ASTM D-695-15 [52] and Kucharek, MacRae e Yang [53]. A texture analyzer (model XTplus, TA instruments) was used on the compressive pattern model, using a

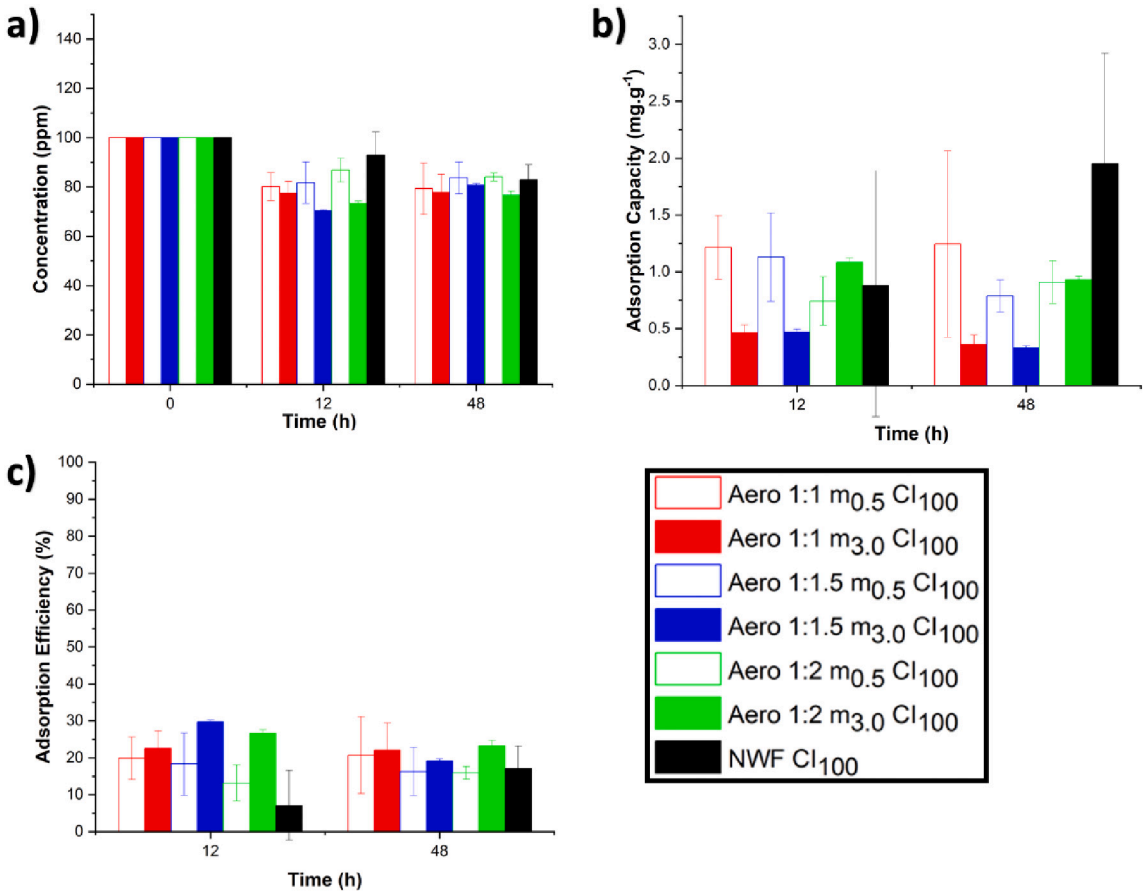

Fig. 8. Results of **a)** concentration (ppm) after adsorption, **b)** adsorption capacity ($mg{\cdot}g^{-1}$), and **c)** adsorption efficiency (%) for systems containing the divalent cadmium ion at an initial concentration of 100 ppm, varying the type of adsorbent and the weight, related to the measured times, respectively.

constant uniaxial compression speed of 1 $mm{\cdot}min^{-1}$, pre-and post-testing speed of 600 $mm{\cdot}min^{-1}$, and a 5 kN load cell. The samples were prepared according to ASTM D-695-15 [52], using the cylindrical sample type with a diameter of 8.4 ± 0.2 mm and height of 10.5 ± 0.5 mm. Thus, the tests were performed on ten samples of each composition, an anisotropic material.

2.3.4. Specific surface area (BET)

The surface area of corn starch and nanocellulose aerogels were investigated by ultra-high purity nitrogen adsorption and desorption isotherms at 77.3 K using the Brunauer, Emmet, and Teller (BET) equation (Quantachrome Instruments, mod. Nova 1200e, Kingsville, TX). Before measurement, approximately 200 mg of the sample was heated at 110–115 °C for 4 h under a vacuum for degassing. For surface area determination, the adsorption isotherms in the linear region of the BET plot (at a relative pressure P/P0 in the range from 0.05 to 1) were used using a multipoint BET [54–56].

2.3.5. Adsorption of cadmium and zinc

The adsorption studies were based on the methodology of batch adsorption experiments as described by Herman, Fábián, and József Kalmár. It consists of dry samples of corn starch aerogels immersed in a solution containing the ion to be removed. This system was kept under a controlled temperature of approximately 25 ± 5 °C and rotation of 120 rpm [57], as presented in Fig. 2.

For in-depth comprehension of the adsorption mechanism of corn starch aerogels, some parameters were chosen as fixed and others as variables, seeking to observe their influences on the adsorption capacity and efficiency [58,59], highlighted in Eqs. (2) and (3), respectively. Thus, concentration measurements were performed by Inductively Coupled Plasma Mass Spectrometry (ICP-MS), using an Agilent Technologies, model 7900 (Hachioji, Japan) instrument to obtain data to find adsorption capacity ($mg \cdot g^{-1}$) and efficiency (%). Cadmium and zinc standards were prepared from a standard solution of these ions (PerkinElmer, Inc., USA) to construct the calibration curve.

$$\text{Adsorption capacity (Q)}\left(mg.g^{-1}\right) = \frac{(C_0 - C_f)}{m_a} \times V_S \; 100\% \tag{2}$$

$$\text{Adsorption efficiency (E)}(\%) = \frac{(C_0 - C_f)}{C_0} \times 100\% \tag{3}$$

C_0 ($mg{\cdot}L^{-1}$) is the initial concentration, C_f ($mg{\cdot}L^{-1}$) is the concentration at each time of withdrawal of the aliquots or the equilibrium concentration, m_a is the adsorbent weight, and V_S is the volume of the adsorption solution containing potentially toxic elements ions.

The temperature of the systems was 25 ± 5 °C, and the agitation was 120 rpm, considered the study's fixed parameters. These parameters were controlled by accommodating the systems in a Shaker Benchtop Incubator with Agitation and Heating (Solab Equipment for Laboratories, model SL-222/E). The other fixed parameters were the ions, the volume of solution used, and the pH of the solutions. The ions investigated were cadmium [Cd(II)] and zinc [Zn(II)]. In addition, the volume of the solution was 100 mL of solution and the constant pH for all ions and at all concentrations tested was approximately 4–5, with a pH previously chosen as fixed due to the good results previously described in the literature [59–61].

In contrast, the variable parameters were the adsorbent weight (g), the initial concentration (ppm), the time (h), and the type of aerogel used. In addition to the systems containing each ion, measurements were carried out without the ion's presence and in the nitric acid

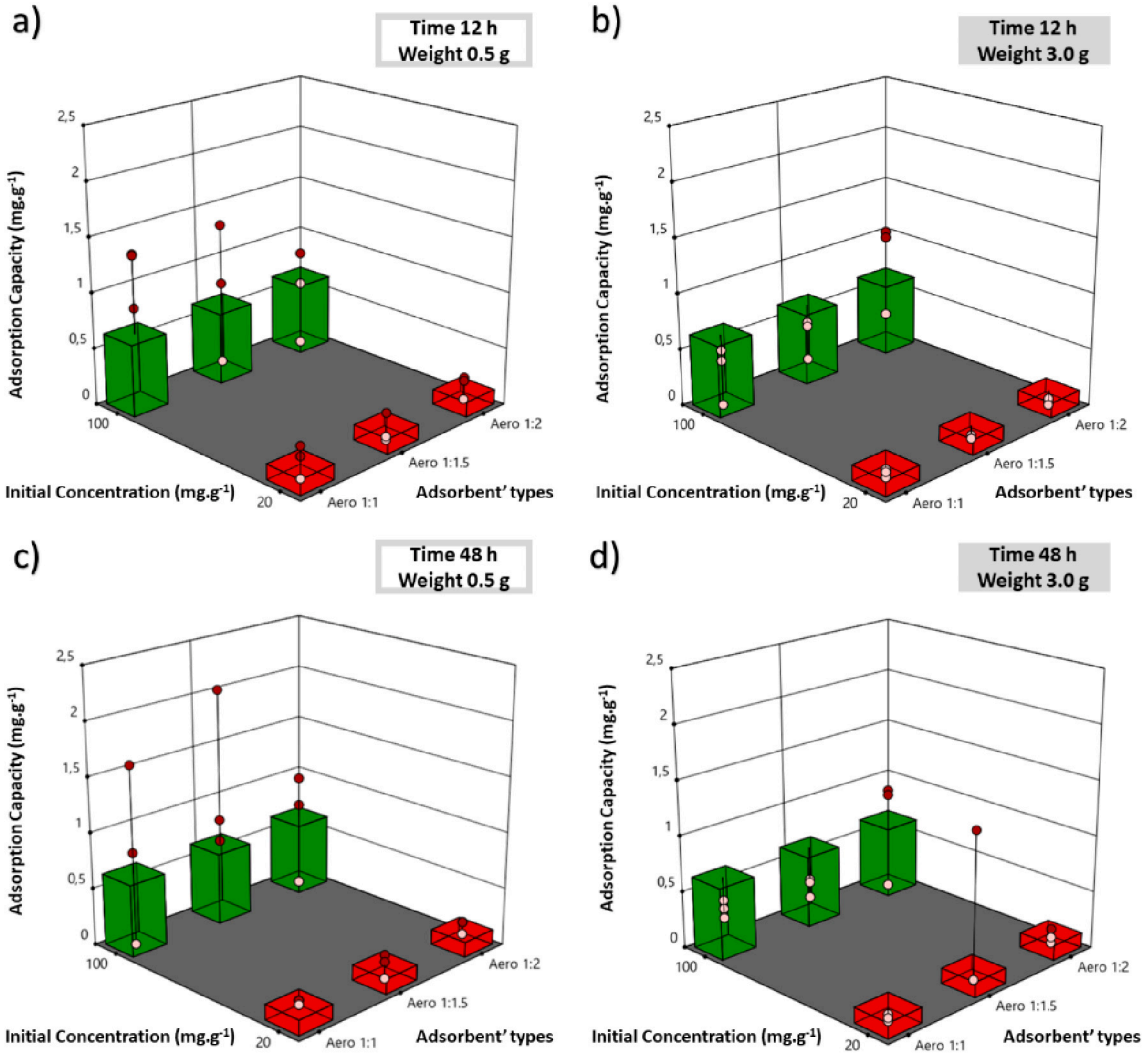

Fig. 9. Multivariate factorial from the design of experiments for the adsorption capacity ($mg \cdot g^{-1}$) of cadmium II, keeping the initial concentration and type of aerogel fixed, and varying the time and the adsorbent weight, corresponding to **a)** time of 12 h of adsorption and 0.5 g of adsorbent weight, **b)** time of 12 h of adsorption and 3.0 g of adsorbent weight, **c)** time of 48 h of adsorption and 0.5 g of adsorbent weight, and **d)** adsorption time of 48 h and 3.0 g of adsorbent weight.

solution. The systems were prepared using *stock* solutions containing each of the ions, at a concentration of 1000 ppm and 200 ppm, with a dilution ratio of 1:9, where 90 mL was a solution of nitric acid (HNO_3) 0.01 M and 10 mL of the stock solution, thus resulting in each system containing 100 ppm and 20 ppm (initial concentration) [57]. The pH adjustment between 4 and 5 was from a 0.1 M sodium hydroxide solution added to each system containing the ions [31]. The time interval for the adsorption was 12 h and 48 h, aiming to evaluate the maximum adsorption time or the equilibrium adsorption [62]. The adsorbent weight was chosen considering a low weight ratio of 0.5 g and extrapolating to 3.0 g of adsorbent [63].

An NWF wrapper (non-woven fabric) was used for packaging the corn starch aerogels, aiming to make prototypes to apply the adsorbents. It is due to possible inertia in the adsorption process, as this type of fabric, in addition to being porous, allows the permeation of the solution for contact with the aerogels, promoting their protection [64,65]. Therefore, the aerogels were sealed inside the NWF wrappers using a Timer Sealer (M30 Sela Bivolt, NK Embalagens).

The adsorption systems containing the ions were named according to the type of aerogel, the adsorbent weight used, and the concentration of the initial used to remove the ions [Aero (ratio starch: crosslinking agent) $m_{(adsorbent\ weight)}$ CI $_{(initial\ ion\ concentration)}$]. As for the samples characterized as Blank systems, the systems without the presence of ions (only acid, base for pH adjustment, and adsorbent) were named by the type of aerogel, and the weight used [Aero (ratio starch: crosslinking agent) $m_{(adsorbent\ weight)}$ Blank]. Moreover, the systems with the ions and the NWF without the aerogel were named NWF CI $_{(initial\ ion\ concentration)}$. Finally, the solutions containing only the acid solution were named Blank HNO_3.

2.3.6. General factorial

For a statistical evaluation of the adsorption capacity (Q) and adsorption/removal efficiency (E) data, their results were treated in the experiment design software (*Design-Expert® Version 11 Software*) using *General Factorial*, previously used to plan the experiments performed. The *Multilevel Categoric* factorial function was used to evaluate the interactions between the variables of aerogel type, initial concentration, adsorption time, and adsorbent weight related to the responses mentioned above in triplicate [66,67]. For factorial evaluation, the 3D surface graphics model was used to exemplify and demonstrate the interactions and differences between the samples to understand the most significant factors, thus showing the best factors that result in better results.

2.3.7. X-ray photoelectron spectroscopy (XPS)

The XPS experiments were conducted on a ThermoFisher Scientific

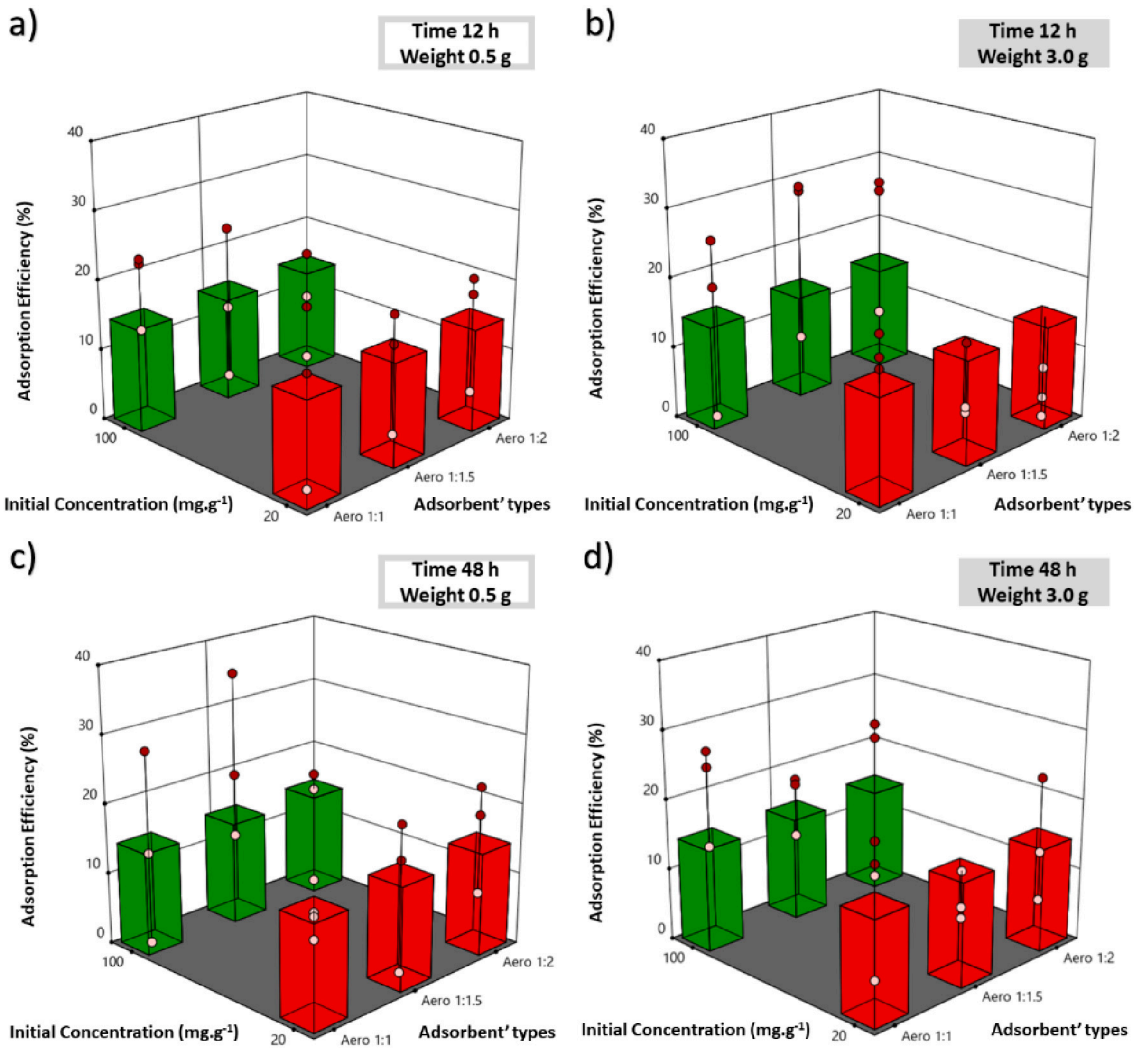

Fig. 10. Multivariate factorial from the design of experiment for the adsorption efficiency (%) of cadmium II, keeping the initial concentration and type of experiments for the adsorption aerogel fixed, and varying the time and the adsorbent weight, corresponding to **a)** time of 12 h of adsorption and 0.5 g of adsorbent weight, **b)** time of 12 h of adsorption and 3.0 g of adsorbent weight, **c)** time of 48 h of adsorption and 0.5 g of adsorbent weight, and **d)** adsorption time of 48 h and 3.0 g of adsorbent weight.

K-alpha + model, with A1 Kα monochrome radiation at room temperature. Spectra were performed with 10 or 20 eV for high-resolution scans. All data were processed in CASAXPS software.

3. Results and discussion

3.1. Structural formation of aerogels

Fig. 3 presents images of the starch aerogels prepared by different crosslinking agent concentrations followed by freeze-drying.

It was verified that all the aerogels presented a visual aspect like an open-cell foam, with apparent roughness, observed in Fig. 3. This appearance of solid foam was verified by Ferreira and Rezende, who prepared ultralight cellulosic materials from cellulose microfibrils isolated from eucalyptus pulp and dried them in a conventional oven [68]. Dogenski et al. also obtained foam-like aerogels with apparent roughness. They reported that the process of gel formation is essential. However, the aqueous medium is also one of the determining factors for forming aerogels with a rigid structure and without collapse [69].

Moreover, one of the essential parameters for the formation of aerogels is the shrinkage rate of aerogels. This aspect is recurrent in the aerogel's drying process as well as in the intrinsic structure of the precursor material. It is generated by forming hydrogen bonds between the macromolecules of the chain structure of the three-dimensional network [70]. Therefore, the Aero 1:1, Aero 1:1.5, and Aero 1:2 samples obtained a shrinkage rate of 20.0 ± 5.0, 11.1 ± 4.0, and 17.0 ± 2.0, respectively.

From the results obtained for all samples, the Aero 1:1.5 sample had the lowest shrinkage rate among the aerogels studied. It indicates the lower impact of the freeze-drying process with an intermediate concentration of the crosslinking agent. Vareda, Lamy-Mendes, and Durães reported that aerogels generally have an acceptable shrinkage rate below 25 %, maintaining their dimensional stability without significant changes due to drying and the formation of hydrogen bonds in organic aerogels [71]. The slight influence of freeze-drying drying on the shrinkage rate compared to supercritical drying, described by Czlonka, shows that the main factor responsible for this aspect is the formation of intermolecular bonds between the polymer chains during crosslinking [70]. Furthermore, let us evaluate the Aero 1:1 and Aero 1:2 samples. A higher shrinkage rate can be correlated with a higher densification of the structure and, therefore, a higher density of the aerogels [72], showing that the sample with a possible lower density is Aero 1:1.5 aerogel. Therefore, all the prepared starch aerogels had a foam appearance, with apparent roughness, without defects or collapsed structure, and still

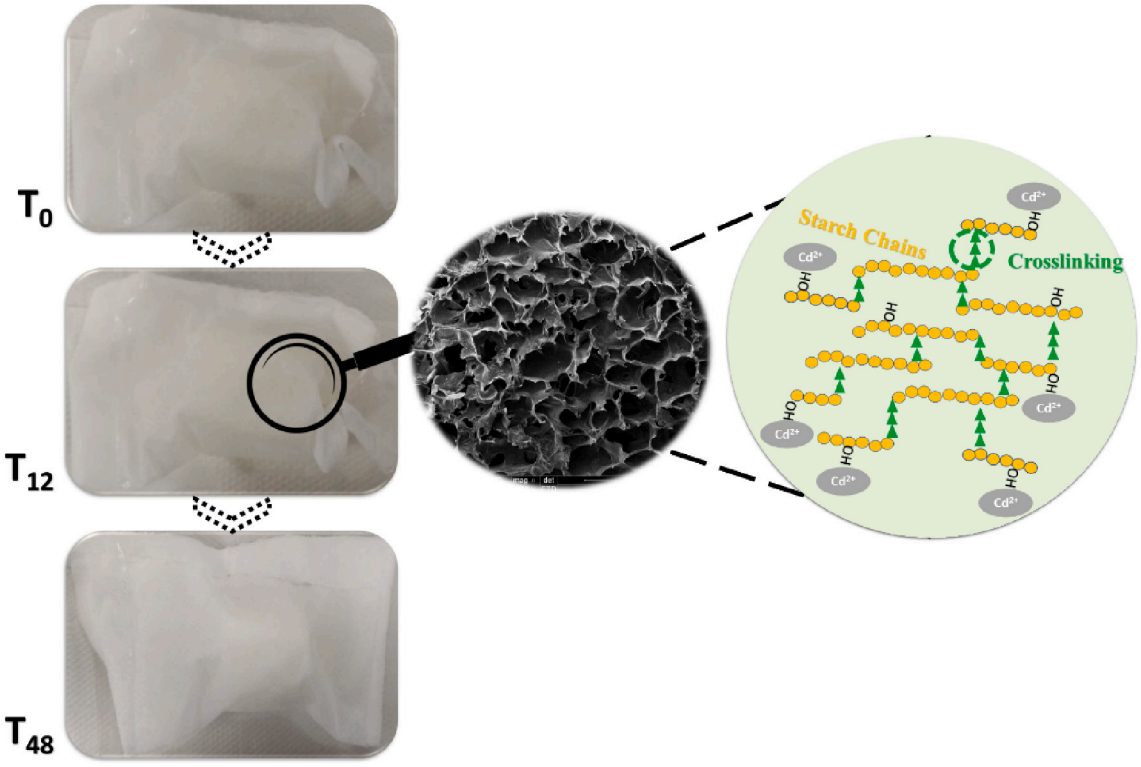

Fig. 11. Visual aspect images at the beginning of the Cd(II) adsorption tests and after 12 and 48 h for the Aero 1:1.5 $m_{3.0}$ CI_{100} sample.

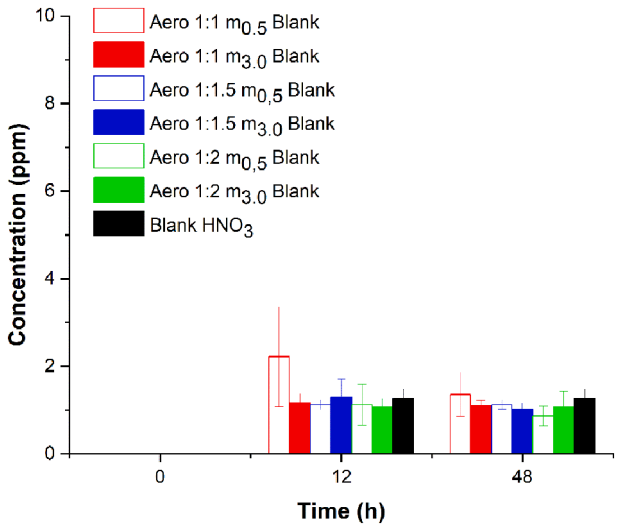

Fig. 12. Concentration (ppm) results after adsorption for the Blank systems and the acidic NaOH solution without the adsorbent related to Zn(II) systems.

with a low shrinkage rate, showing the efficiency of the aerogel's structure obtaining.

3.2. Mechanical compressive analysis

Fig. 4 presents the stress-strain curves for three aerogel types, evaluating the mechanical compressive performance.

The behavior of the stress-strain curves presented in Fig. 4 is classified as typical curves of a bioaerogel. It is corroborated by Buchtová et al., who verified that the stress-strain curves for bioaerogels contain a linear elastic region at low strains, allowing the determination of the modulus of elasticity, and showing a stress plateau, corresponding to a progressive buckling of the cell walls, and densification of the material at high strains, where the stress abruptly increases [73]. Ganesan et al. also observed the exact behavior of the stress-strain curves for cellulose aerogels [74]. Besides, from the stress versus strain curves in Fig. 4, Table 1 presents the results of compressive modulus, maximum compressive strength, and strain strength at 5, 10, and 20 % (kPa), as well as the maximum strain at compression (%).

Evaluating the compressive modulus results highlighted in Table 1, the sample that presented the highest value of compressive modulus was the Aero 1:2, with 123.0 ± 4.0 kPa. It was possibly due to the increase in the crosslinking agent concentration, resulting in a higher cell density, which generated a high compressive modulus. Wang et al. presented that increased compressive modulus is possibly due to the formation of structures with higher crosslink density, which can dissipate energy more effectively under applied stress [75].

Regarding the maximum compressive strength (kPa), according to the increase in the crosslinking agent concentration, there was a decrease in the compressive strength value. This phenomenon may have occurred due to the influence of pore size. As previously discussed in previous results [47], the difference in pore size values between the Aero 1:1 and Aero 1:2 samples for the most prominent pores was 163.4 μm, and for the smallest pores, it was 14.4 μm; thus, the Aero 1:2 sample performed the highest values of macropores. Ganesan et al. claim that smaller pore sizes result in higher mechanical strength than larger pores [74]. In contrast, Wu et al. observed that larger pores lower aerogel compressive strength and elasticity [76], justifying the previous affirmative. Furthermore, this statement supports the higher pore density value of 54.3 cont. mm^{-2}, which was 1.5 times greater than the pore density of the Aero 1:1 sample and 9.7 times higher than the Aero 1:2 sample [47].

The same trend of the maximum compressive strength values was observed for the maximum strength values at 5, 10, and 20 %, showing a slight difference between the samples but still supporting a greater degree of crosslinking for the Aero 1:2 sample allowing a higher value of mechanical strength. The same crosslinking trend and increase in these

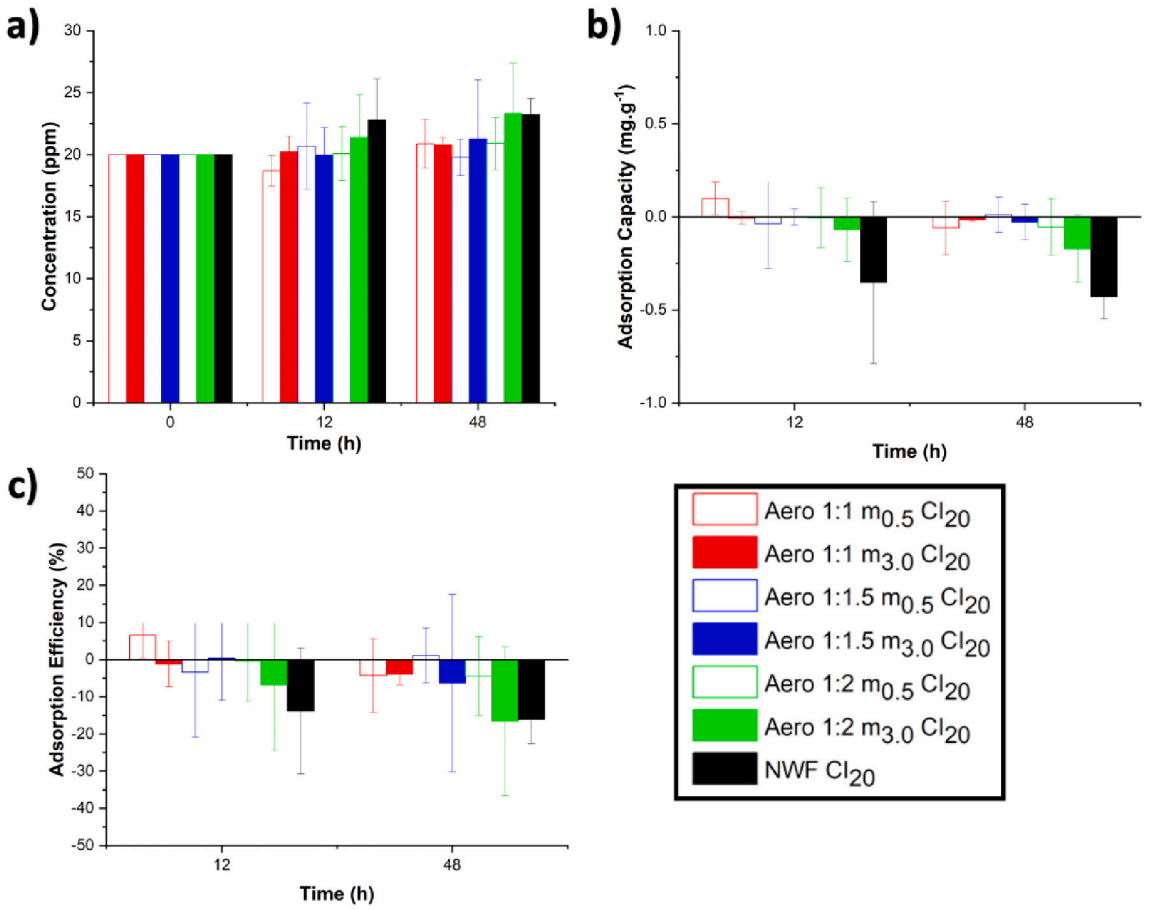

Fig. 13. Results of **a)** concentration (ppm) after adsorption, **b)** adsorption capacity ($mg{\cdot}g^{-1}$) and **c)** adsorption efficiency (%) for systems containing the divalent zinc ion at an initial concentration of 20 ppm, varying the type of adsorbent and the weight, related to the measured times, respectively.

values were observed in the work of Zhao, Tian, and Huang. They evaluated these results and increased aerogel strength as the degree of crosslinking of clay-reinforced starch aerogels increased [77]. Wang et al. obtained excellent mechanical properties due to a higher crosslinking degree. It was due to the higher degree of crosslinking and interlacing of the polymer chains, which are associated with a higher percentage of crosslinking agents, thus forming an ordered and stable three-dimensional crosslinking agent structure [78].

Another influence on the mechanical strength of aerogels was described in previous work. The degree of crosslinking observed by the ratio of 1582/995 cm^{-1} peaks associated with crosslinking increased by 73 % between samples Aero 1:1.5 and Aero 1:1, and 12 % between Aero 1:2 and Aero 1:1.5 samples, correlating with the increase of mechanical performance of these samples. The increase in water absorption confirmed this association with the increased crosslinking of the system because the lower the water absorption, the more the structure is crosslinked due to the decrease in the movement of the chains for water permeation in its structure [47]. Therefore, there was a slight increase in the maximum strain at compression, corroborating the decrease in the maximum compressive strength values. It was caused by the collapse of the pore walls due to the decrease in the amount of force that the sample resists [79], showing that intermediate concentrations of crosslinking agent (Aero 1:1.5) are better at maintaining the mechanical properties of starch aerogels.

3.3. Specific surface area (BET)

One of the main characteristics that make aerogels a promising candidate for applications, as in the case of adsorption, is the surface area. According to Ganesan et al., starch aerogels have a surface area ranging from 100 to 400 $m^2{\cdot}g^{-1}$ [80]. The BET (Brunauer–Emmett–-Teller) method consists of the adsorption/desorption of nitrogen under pressure to characterize the surface area, pore size, and pore volume [81]. Therefore, Fig. 5 shows the nitrogen (N_2) adsorption/desorption isotherm graphs of the starch aerogel samples, varying the concentration of the crosslinking agent.

According to Thommes et al., in their IUPAC technical report, they present the adsorption/desorption isotherms of nitrogen, classifying them according to the design of the curve. Therefore, from the appearance of the isotherm curves in Fig. 5, all samples presented a typical type II isotherm curve. It corresponds to the physisorption of most gases in nonporous or macroporous adsorbents [81]. The design of the isotherm curve is connected to what was observed in the results of scanning electron microscopy regarding the mean pore size in previous work [47]. Da Costa et al. also observed BET's exact design of nitrogen adsorption isotherm curves, classifying their natural biocomposites based on sericin/alginate/poly(vinyl alcohol). They observed a tendency towards a macroporous structure due to obtaining a type II isotherm curve of its material, aiming at the recovery of ytterbium in a packed bed column [82]. In addition, Wang et al. investigated the effect of supercritical drying methods using CO_2 and freeze-drying using liquid nitrogen to prepare cellulose nanofibrils (CNF) aerogels. They observed that their aerogels had an isotherm curve design for freeze-drying, like type II. However, observing a small number of micropores and mesopores in their aerogel structure formed due to the slow rise at small, applied pressures [51].

Table 2 shows the average values of BET-specific surface area, pore diameter, and pore volume obtained for the corn starch aerogels,

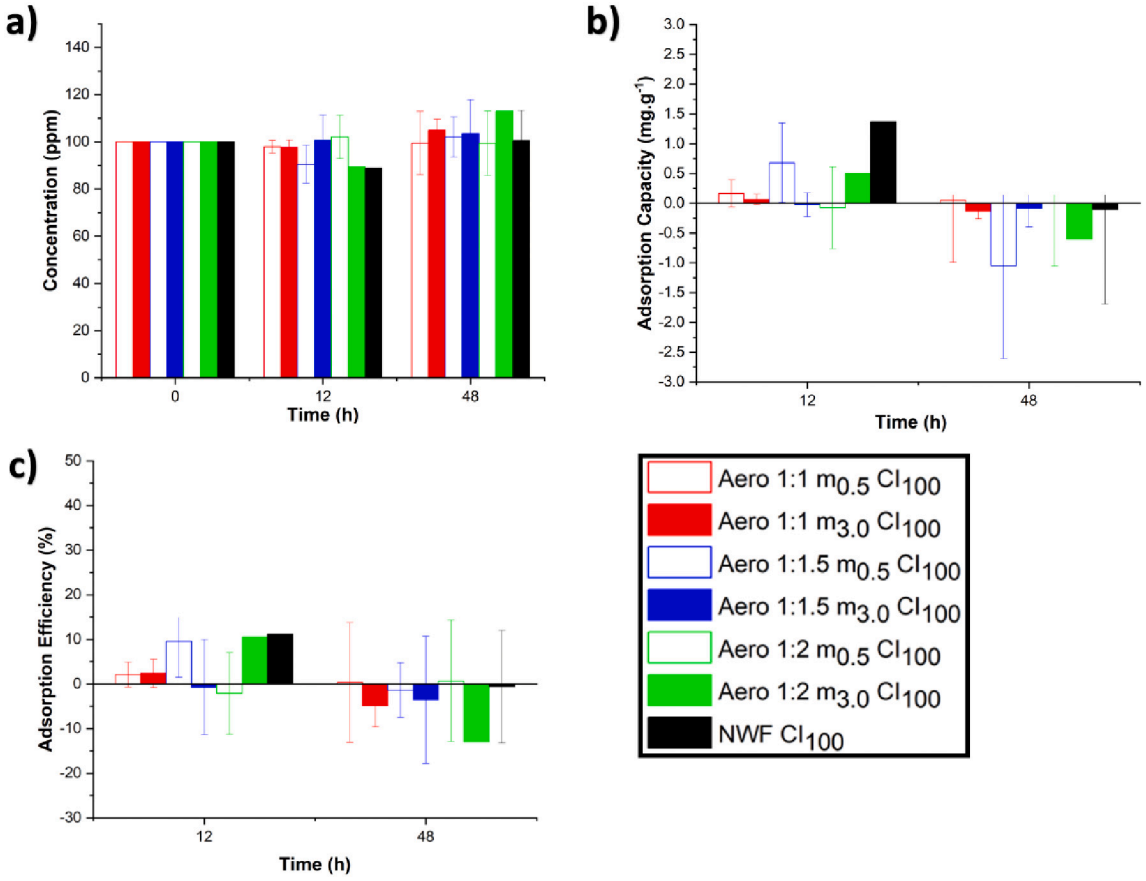

Fig. 14. Results of **a)** concentration (ppm) after adsorption, **b)** adsorption capacity ($mg{\cdot}g^{-1}$), and **c)** adsorption efficiency (%) for systems containing the divalent zinc ion at an initial concentration of 100 ppm, varying the type of adsorbent and the weight, related to the measured times, respectively.

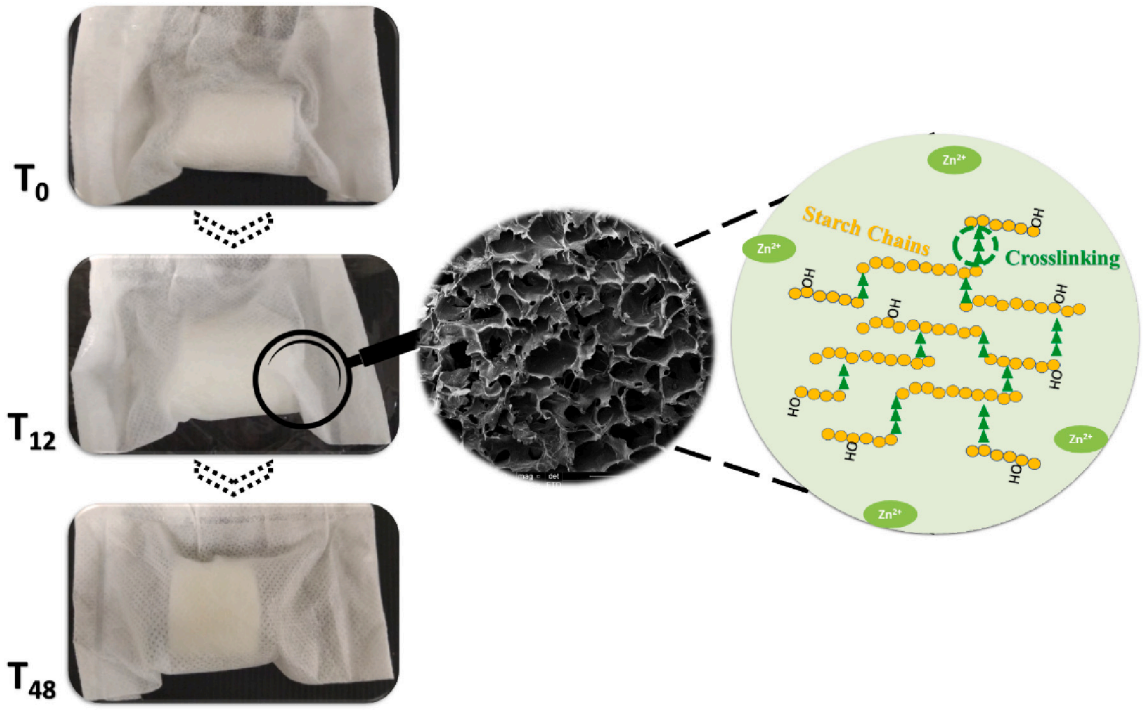

Fig. 15. Visual aspect images at the beginning of the Zn(II) adsorption tests and after 12 and 48 h for the Aero 1:1.5 $m_{3.0}$ CI_{100} sample.

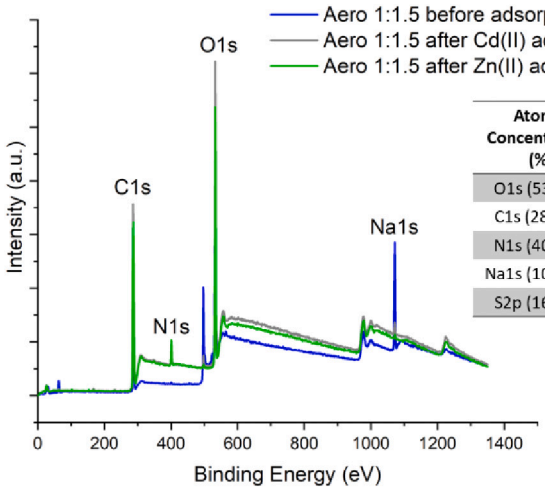

Atomic Concentration (%)	Aero 1:1.5 before adsorption	Aero 1:1.5 after Cd(II) adsorption	Aero 1:1.5 after Zn(II) adsorption
O1s (534 eV)	37.4 ± 2.0	33.6 ± 3.0	31.6 ± 1.0
C1s (284 eV)	44.5 ± 1.0	63.3 ± 2.5	62.4 ± 1.5
N1s (401 eV(	1.2 ± 1.0	2.0 ± 0.3	5.1 ± 1.0
Na1s (1072 eV)	16.8 ± 0.4	1.0 ± 0.2	0.3 ± 0.1
S2p (168 eV)	----	0.2 ± 0.1	0.6 ± 0.1

Fig. 16. XPS survey spectra for Aero 1:1.5 before adsorption, and the Aero 1:1.5 $m_{3.0}$ CI_{100} sample after adsorption of Cd(II) and Zn(II), and atomic concentration for their samples, respectively.

corroborating the design of the nitrogen adsorption/desorption isotherm curves.

It is observed that the Aero 1:1 sample had a higher surface area compared to the other samples. Furthermore, as the concentration of crosslinking agent increased, a decrease in surface area and pore volume was observed. According to Ganesan et al., the BET method for evaluating the surface area of polysaccharide aerogels, or bio-aerogels, is limited due to the contraction the structure may undergo due to the type of precursor molecule employed. In the case of polymers formed by glycosidic units and with a high presence of crosslinks, there may be, in addition to contraction and shrinkage, the formation of macropores [80], that is, evaluating the results of the pore sizes by scanning electron microscopy, the apparent density and the percentage of shrinkage, the Aero 1:1.5 sample is still more promising than the other samples due to the low shrinkage it has suffered after drying by freeze-drying, obtaining a less dense structure, with the presence of macropores observed by SEM and micropores obtained by BET, with a good pore density and the lowest density.

3.4. Adsorption of cadmium and zinc

3.4.1. Adsorption capacity and efficiency of Cd(II) from starch aerogels

Fig. 6 presents the concentration results for Blank systems without the Cd(II) related to the results obtained by the ICP-MS.

First, evaluating the concentration results of Fig. 6 obtained for the Blank systems, without the presence of Cd(II), containing the adsorbent and without its presence (Blank HNO_3), there was a tiny presence or trace of the ions in these systems because the concentration is close to or equal to 0 ppm. Therefore, it was proved that the non-interference of this ion through contamination of the systems could generate an analytical error in the systems with the presence of the ion. In addition, the integrity of the adsorbents in the acidic medium was observed, so they were not adsorbed.

Proving the non-interference of the systems without the presence of cadmium ion, Fig. 7 present the results from the systems with the addition of divalent cadmium ions, with 20 ppm initial concentration, highlighting concentration (ppm), adsorption capacity ($mg \cdot g^{-1}$) and efficiency (%), respectively.

For systems at 20 ppm Cd(II) concentration, Fig. 7.a shows the results at 0, 12, and 48 h. After 12 h of adsorption, all samples showed a slight decline in final concentration. Their respective deviations and analytical errors were minor for samples containing NWF and starch aerogel. However, the same behavior was the opposite for the system that contained only the NWF (without the presence of the starch aerogel), showing an imprecision and a significant analytical deviation. Possibly the NWF (non-woven fabric), made of polypropylene, only absorbed the content on its surface (in some cases) but without complete adsorption due to the wettability of its fibers by water. Wei et al. stated that NWF made of PP could be used for the adsorption of metals due to its characteristics such as disordered fiber structure, high specific surface, low cost, and degradable nature. However, due to its hydrophobicity and inert chemical structure, it resulted in low affinity with water and metals' adsorption, compromising the metal ions' adsorption aspect and thus requiring a surface modification of these fibers [65]. In the case of the adsorbent prototype (NWF and starch aerogel), no modification of the NWF was carried out, thus proving the non-adsorption of cadmium in the fibrillar structure of the NWF and allowing the textile and fibrillar bioriented structure of the NWF to make it feasible for the permeation of contaminated water to enter contact with the aerogel.

For the adsorbent prototypes, concentration results for all aerogel samples showed a removal between 2 and 4 ppm, resulting in a small removal of cadmium II ions when the initial concentration was lower (20 ppm). The same trend was observed for the adsorption capacity results ($mg \cdot g^{-1}$), with a small variability for all aerogels. However, comparing the weight of the adsorbent used (0.5 and 3.0 g, respectively), the lower weight of the adsorbent resulted in a higher adsorption capacity. Lei et al. also observed the same phenomenon in the adsorption of cadmium II on highly stable dopamine-modified magnetic nanoadsorbents. They observed that if the initial concentration and volume of cadmium are constant, the number of cadmium ions in contact with the surface of the adsorbent per unit weight decreases with the increasing dosage of the adsorbent [83].

As for the adsorption time, both adsorption capacity and efficiency were influenced. A shorter adsorption time of 12 h was more satisfactory than 48 h. The equilibrium adsorption time occurred in 12 h, with a shorter adsorption time due to the appropriate forces produced for mass transfer between the solid and liquid phases, as described by Zadeh, Esmaeili, and Foroutan [84]. Compared with other adsorbents, such as polyethylene microspheres, which obtained a maximum adsorption capacity of 0.01 $mg \cdot g^{-1}$ between 12 and 48 h [85], the Aero 1:1 sample and adsorbent weight of 0.5 g obtained an adsorption capacity of 0.2 ± 0.1 $mg \cdot g^{-1}$ and adsorption efficiency of 21.0 ± 6.2 %. It demonstrates higher adsorption efficiency of corn starch aerogels than the adsorbents described in the literature. In contrast, Fig. 8 presents the results of the 100 ppm initial concentration, regarding concentration (ppm), adsorption capacity ($mg \cdot g^{-1}$), and efficiency (%), respectively.

In general, increasing the initial concentration from 20 ppm to 100 ppm, there was a sudden decrease in concentration after 12 h, steadying

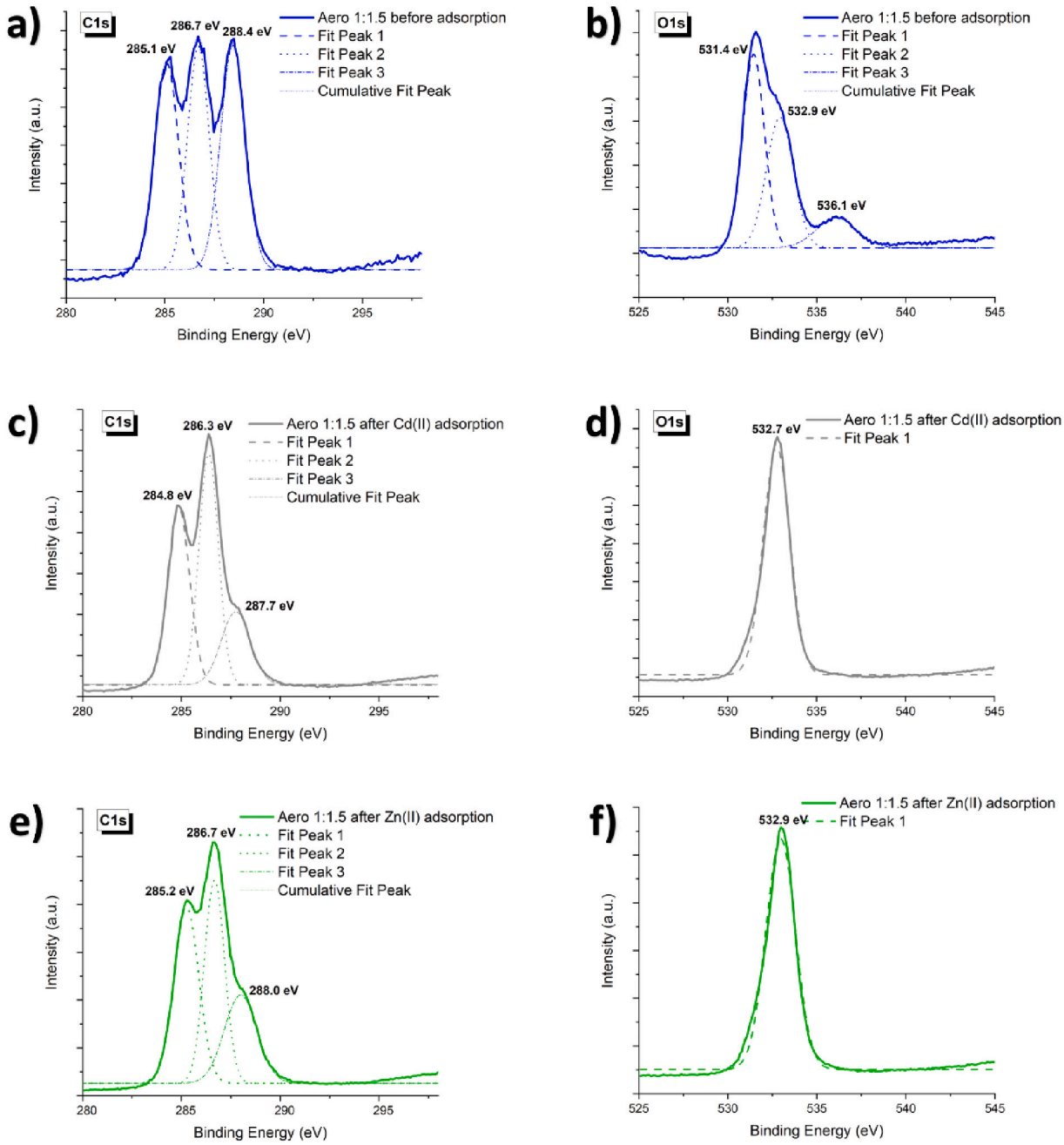

Fig. 17. C1s and O1s spectra for a) and b) Aero 1:1.5 before adsorption, and the Aero 1:1.5 $m_{3.0}$ CI_{100} sample after adsorption of c) and d) Cd(II), and e) and f) Zn(II), respectively.

until 48 h. Evaluating only NWF samples, such as TNT CI_{100}, low adsorption values, and high adsorption capacity and efficiency, following the same trend of high deviations as the 20 ppm initial concentration samples.

In the adsorbent prototypes, a concentration decrease between 20 and 30 ppm for 100 ppm initial concentration samples was found, affecting higher adsorption capacity and efficiency. Awual et al. verified the same trend of values that indicated a possible application for this purpose. On the other hand, to use this adsorbent remediation contaminated environments with a high concentration of cadmium ions [86]. It is likely due to the increase in driving force, i.e., the stronger concentration gradient at the higher concentration, thus driving the Cd (II) ions to the surface of the adsorbent [87]. Then, it resulted in a more effective removal of Cd(II) ions from the surface of the aerogel. Besides, a higher adsorbent weight (3.0 g) resulted in higher cadmium removal. This effect is contrary to the result presented in the weight of 0.5 g. Bakole et al. obtained the same result for Cd(II), investigating the adsorption of the potentially toxic elements using two different nano-adsorbents: purified carbon nanotubes and polyhydroxybutyrate functionalized carbon nanotubes [88]. Thus, the general factorial from DOE evaluation proved the previous conclusions, analyzing adsorption capacity and efficiency. Four variables were chosen, X1 (adsorbent type) and X2 [initial concentration ($mg{\cdot}g^{-1}$)] as fixed variables on the X axis, to observe the results of adsorption capacity (Fig. 9) and adsorption efficiency (Fig. 10) in the Y axis. Besides, the adsorption time (12 and 48 h) and the adsorbent weight (0.5 and 3.0 g) were varied.

From the results of the general factorial obtained by the 3D surfaces, for the adsorption capacity response, the initial concentration of 100 ppm presented superior results than the adsorption capacity results of the initial concentration of 20 ppm, proving what was discussed

Table 3
Peak areas for C1s and O1s spectra for Aero 1:1.5 before adsorption, and the Aero 1:1.5 $m_{3.0}$ CI_{100} sample after adsorption of Cd(II) and Zn(II), respectively.

Peak area	Samples		
	Aero 1:1.5 before adsorption	Aero 1:1.5 after Cd(II) adsorption	Aero 1:1.5 after Zn(II) adsorption
Peak 1 – C1s (C—C and C—H bonds)	1.7×10^{10}	2.5×10^{10}	2.3×10^{10}
Peak 2 – C1s (C—OH and C—O—C bonds)	9.6×10^{9}	2.8×10^{10}	2.7×10^{10}
Peak 3 – C1s (O—C═O bonds)	1.7×10^{10}	1.7×10^{10}	2.1×10^{10}
Peak 1 – O1s (C═O bonds)	7.3×10^{10}	–	–
Peak 2 – O1s (O—H bonds)	3.6×10^{10}	9.8×10^{10}	1.0×10^{10}
Peak 3 – O1s (C—O bonds)	8.6×10^{9}	–	–

previously. Islam et al. also observed this trend, in which they found that Cr(VI) sorption increased with increasing o Cr(VI) ion concentration [89]. Consequently, a higher initial concentration generates more significant removal of contaminants, indicating the possible applicability of these adsorbents for remediation of environments with high content of contaminants.

There was a slight difference between the two initial concentrations, analyzing the adsorption efficiency results, and there is not a very significant difference between the adsorption efficiency of the aerogel types. Besides, higher-weight aerogel (3.0 g) generated better results, as observed in Fig. 10.b and d, respectively. Hasanpour and Hatami reported that the high percentage removal of potentially toxic elements increases quickly with an increase in the dosage of adsorbents due to greater accessibility of the surface area and exchangeable sites [90]. In contrast to Naushad et al., they correlated the decrease in the adsorption capacity and the aggregation of para-aminobenzoic acid functionalized activated carbon sites, which increased adsorbent and decreased the total surface area [91]. Thus, a more porous adsorbent weight generates more available active sites, improving metal ion removal.

On the other hand, evaluating the average results of the adsorption capacity and efficiency, as well as the evidence of the interactions between the factors evaluated by the 3D surface obtained by the DOE, among these results, the sample Aero 1:1.5 $m_{3.0}$ CI_{100}, with 12 h contact time have obtained better results. Higher values of adsorption capacity (0.47 ± 0.03 mg·g^{-1}) and adsorption efficiency (30.0 ± 0.5 %) were obtained. It agrees with data obtained in previous studies by Camani et al. The sample Aero 1:1.5 presented larger average pore sizes (180.7 ± 41.1 μm) and smaller (33 ± 11 μm) that were lower than the other crosslinking agent concentrations (Aero 1:1 and Aero 1:2) [47]. Furthermore, a higher porosity (90 %) and high specific surface area (198.0 $m^2 \cdot g^{-1}$) were found in this sample. Liu et al. found that smaller pores promote excellent retention and adsorption capacity than samples with larger pore size distribution [92]. Zhou et al. claim that high porosity and water permeability (generated by the material's affinity for water) can promote greater metal ion diffusivity in the hydrogel structure [93]. Besides, Rahman et al. correlated the high detection, absorption, and adsorption capability of 3-methoxyanaline (3-MA) due to the large surface area of porous nanocomposite formed by a thin layer of $Ag_2O_@La_2O_3$ NSs into glassy carbon electrode [94].

Lastly, hydroxyl groups generate the cation-π interactions between -OH and cadmium ions, resulting in possible more complexation and higher adsorption [95,96]. Kubra also associated the Cu(II) removal with the complexation bonding with functional groups present into 4-dodecyl-6-((4-(hexyloxy)phenyl)diazenyl)benzene-1,3-diol (DPDB) ligand of composite material based on mesoporous silica monoliths [97]. However, Aero 1:1.5 obtained the best result due to the availability of hydroxyl groups [98] and high surface area, which promoted hydrogen bonds interacting with Cd(II). Then, Fig. 11 presents visual aspect images of the Aero 1:1.5 $m_{3.0}$ CI_{100} sample at the T_0, T_{12}, and T_{48} of the Cd (II) adsorption tests and the scheme explaining the adsorption mechanism.

Therefore, higher porosity, high specific surface area, hydroxyl groups, smaller pore sizes, higher initial ion concentration, and higher adsorbent weight promote more significant adsorption of the Cd(II) ion, as shown in Fig. 11, illustrating the visual aspect images. At T_0, as well as after T_{12} and T_{48}, in addition to a proposal on how the adsorption of cadmium ions on the aerogel surface occurs.

3.4.2. *Adsorption capacity and efficiency of Zn(II) from starch aerogels*

Starch aerogels were evaluated as adsorbents for zinc ion [Zn(II)] adsorption systems. Thus, Fig. 12 shows the concentration results for Blank systems without the Zn(II).

Evaluating Fig. 12, the same trend for the Blank systems (without the contaminating ion) with Cd(II) was observed for the systems with Zn(II). In this way, it was possible to verify that there was no interference of this ion through the contamination of the adsorption systems, thus allowing a minor analytical error in the ion systems. Thus, Figs. 13 and 14 evaluate the adsorption systems with Zn(II) ions, presenting the concentration results and adsorption capacity and efficiency for the initial concentration of 20 and 100 ppm, respectively.

In contrast to the bivalent cadmium ion, the Zn(II) adsorption, both for the NWF CI_{20} (Fig. 13) and NWF CI_{100} (Fig. 14) samples, showed the non-affinity of Zn(II) ions with PP fibrillar structure of the non-woven

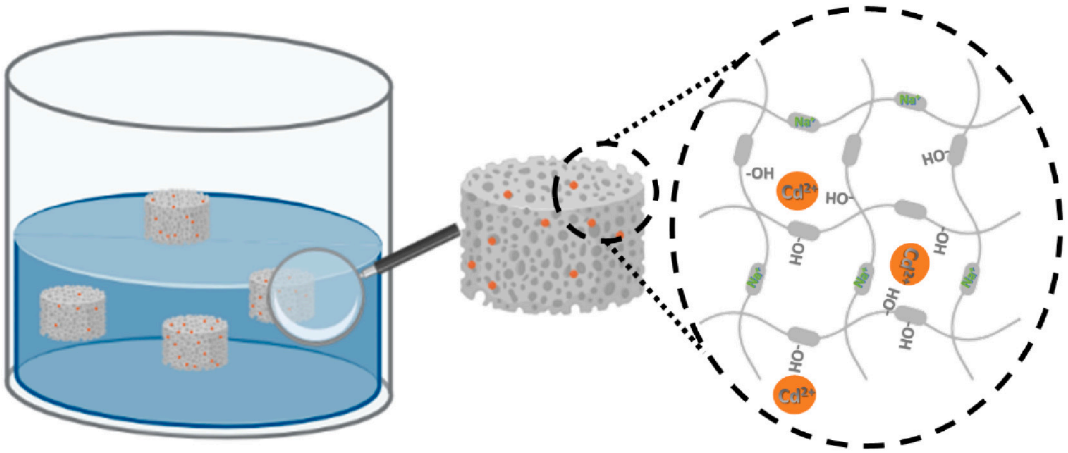

Fig. 18. Possible adsorption mechanism of starch aerogel related to Cd(II) ions.

fabric. The same behavior was observed for prototype samples containing corn starch aerogels. Both concentrations of 20 ppm and 100 ppm presented no adsorption since the final concentration, the adsorption capacity, and the adsorption efficiency obtained results lower than 0, negligible, and even harmful.

Wang et al. claim that the decrease in Zn(II) adsorption capacity is lower for pH less than 6. It is due to decreasing the electrostatic repulsion between the adsorbent and Zn ions at a pH close to 6 [99]. It may be one of the justifications for the non-existent adsorption of Zn(II) ions on the surface of corn starch aerogels. Another explanation that can be reported to support the non-adsorption of Zn(II) ions by corn starch aerogels is the preference of the divalent zinc ion for functional groups such as amine and carboxyl instead of the hydroxyl groups present in the structure of corn starch aerogels. Anirudhan et al. investigated the adsorption of Cu(II) and Zn(II) ions from aqueous solutions using aminoxylated polymerized banana stem (APBS) as an adsorbent. They observed that the complexation of the Zn(II) ion occurred at active sites that contained amine functional groups originating from the structure of the synthesized adsorbent [100]. This hypothesis can be found in more recent works, such as those by Dardouri et al., who investigated the adsorption of Zn(II), Cd(II), and Fe(III) using modified polystyrene with amine groups, with subsequent crosslinking using 2,2′-dichlorodiethyl ether, followed by tris-(2-chloroethyl)-phosphate. They found that the high adsorption selectivity of Fe(III) and Zn(II) ions can be explained by their high affinity with the oxygen and amino acid atoms of the diethyl ether and organophosphate groups [101].

Moreover, Fig. 15 presents the images of the visual aspect after the adsorption process and a scheme of the non-adsorption of zinc ions in the crosslinked structure of corn starch aerogels.

Therefore, the concentration of intermediate crosslinking agent (Aero 1:1.5) showed a higher degree of crosslinking, smaller pore sizes, and higher density of smaller pores, lower density, and higher porosity, as seen in previous work. However, in this paper, this crosslinking concentration (1:1.5) showed a porous structure with a low shrinkage range, a high specific surface area, better adsorption capacity adsorption of cadmium ion [Cd(II)], and better mechanical performance at the concentrations studied (Aero 1:1 and Aero 1:2).

The adsorption time of 12 h showed more conclusive results, possibly being the time to reach equilibrium adsorption, proven by the increase in concentration values after 48 h. The adsorbent weight of 3.0 g showed better values, possibly due to the increase in the available area and contact surface of aerogel, whose Aero 1:1.5 sample showed better values, reaching an adsorption efficiency of 30.0 %. The Aero 1:1.5 sample obtained lower density, higher porosity, smaller pore sizes, and higher pore density than the other samples, resulting in a high specific surface area.

3.4.3. Adsorption mechanism comprehensive

From adsorption results obtained by ICP-MS analysis and multivariate factorial design of experiments (DOE), Aero 1:1.5 was the highest adsorption between all samples. Thus, XPS analysis was performed to evaluate the binding energy modifications, seeking to understand the possible adsorption mechanism for this porous material. Then, Fig. 16 presents the XPS survey spectra of Aero 1:1.5 before adsorption, the Aero 1:1.5 $m_{3.0}$ CI_{100} sample after adsorption of Cd(II) and Zn(II), and atomic concentration for their samples, respectively.

In the survey spectra, all samples - before and after adsorption – presented atomic species as C1s, O1s, N1s, and Na1s, corresponding at 284 eV, 534 eV, 401 eV, and 1072 eV, respectively [102]. Besides, it is observed that the same trend of peaks comparing Aero 1:1.5 before and after adsorption of Cd(II) and Zn(II), with the appearance of two peaks of S2p at 168 eV and N1s at 400 eV. These peaks may be unconsidered due to low atomic percentage after Cd(II) and Zn(II) adsorption. However, Na1s at 1072 eV obtained higher atomic concentration before adsorption due to aerogel synthesis, in which sodium hydroxide is used to generate trisodium citrate, which is the crosslinking agent of this crosslinked structure. As sodium is part of the crosslinking agent chain that participates in the crosslinking, the available sodium ions may have decreased in concentration after adsorption, as these ions may have been released in the aqueous solution containing the ions. Thus, it generated an availability of interaction of the Cd(II) and Zn(II) ions to sites that once interacted with Na ions. Ma et al. reported the same behavior due to the presence of Na ions in the zeolite structure [103]. Another fact to prove this hypothesis was a pH increase after Cd(II) adsorption, from 5.0 to 8.0, showing the influence of Na ions on the aqueous solution, generating NaOH, which increased the media pH. Evaluating XPS spectra for C1s and O1s species in Fig. 17, some considerations for the adsorption process are found. Then, Table 3 denotes the peak areas for each C1s and O1s species, respectively.

Regarding C1s and O1s spectra of samples before and after Cd(II) and Zn(II) adsorption (Fig. 17), the C1s spectra for two steps presented the three peaks. Before adsorption (Fig. 17.a), peak 1 is located at 285.1 eV, 2 at 286.7 eV, and 3 at 288.4 e V, which are associated with C—C and C—H bonds, C-OH and C—O—C bonds, and O—C═O bonds, respectively [104]. After Cd(II) and Zn(II) adsorption (Fig. 17.c and e), these peaks were shifted for low values than Aero 1:1.5 before adsorption. This chemical shift of the C element may be regarded as an adsorption process, in which carbon groups participate the interaction with Cd(II) and Zn(II) [105], in which Zn(II) may have had a small interaction, proved by ICP-MS results.

For O1s spectra, before adsorption (Fig. 17.b), some peaks were observed, as 531.4 eV, 532.9 eV, and 536.1 eV, in which these peaks are related to C═O, O—H, and C—O bonds, respectively [104]. After Cd(II) and Zn(II) adsorption, peak 1 (531.4 eV) and peak 3 (536.1 eV) disappeared from the spectra, maintaining peak 2 at 532.9 eV for Zn(II) adsorbed aerogel sample and shifted this peak for Cd(II) adsorbed aerogel sample. According to Wang, Zhu, and Wang, a decrease in the peak area ratio of C═O and C—O bonds was verified, whereas the peak area ratio of O—H increased. This decrease is linked to the complexation of heavy metal, in which O atoms donate electrons to heavy metal ions, resulting in an electron density of O decrease [104].

Comparing the peak area for C1s and O1s species found in Table 3, C—OH and C—O—C bonds had a significant decrease in this peak area, and O—H bonds presented an increase, especially for Aero 1:1.5 after Cd (II) adsorption, proving the ICP-MS, due to the highest adsorption than Zn(II) ion. Vieira et al. have also observed increased C1s bond intensity due to interaction with Cr(VI) ion [106]. In addition to the possible chemical adsorption observed by the XPS, the pore size observed in the previous work may be one of the factors to help the Cd(II) adsorption. As mentioned above, Aero 1:1.5 presented large average pore sizes (180.7 ± 41.1 μm) and pore density (37.4 cont. mm^{-2}). However, it presented the lowest small pore size (33 ± 11 μm), the highest pore density (54.3 cont. mm^{-2}), and an excellent specific surface area (198 $m^2 \cdot g^{-1}$) [47]. Faghihian, Nourmoradi, and Shokouhi reported that the pore size, pore distribution, surface area, and surface chemistry of the adsorbent contribute to improving the adsorption process [107]. Hao et al. related the action of small pore size to facilitate the copper ion adsorption due to the formation of active sites coordination between copper ion and graphene oxide/montmorillonite composite aerogel [108]. Lastly, Awual et al. obtained Co(II) removal of contaminated water due to the large pore volume and high surface area of the mesoporous inorganic silica [109]. Therefore, as seen in Fig. 18, hydroxyls and carbon-based groups decrease the Na^+ ion number of trisodium citrate after adsorption. Still, the presence of the smallest pore size and high pore density of starch aerogel with intermediate crosslinking agent concentration acted slightly on the adsorption mechanism to Cd(II) for Zn(II).

4. Conclusions

This study focused on the influence of different crosslinking agent concentrations and adsorption conditions on the corn starch aerogels' performance regarding the adsorption of Cd(II) and Zn(II) ions,

structural characteristics such as visual aspect and shrinkage rate, specific surface area, and their mechanical performance. For the adsorption of Cd(II) ions, more significant adsorption was observed for the systems prepared with an initial concentration of 100 ppm than 20 ppm. It was statistically confirmed by the general factorial obtained in the 3D graphs of the DOE. It is due to the increase in driving force, on the other hand, the stronger concentration gradient from the higher concentration (100 ppm).

From the general factorial evaluation obtained by DOE and the adsorption capacity and efficiency results, the Aero 1:1.5 sample, with the adsorbent weight of 3.0 g and from an initial concentration of 100 ppm, presented the best Cd(II) removal performance. A high specific surface area was found by porous structures, considering greater porosity and smaller pore size, that corroborated an improvement of capacity and efficiency of adsorption of Cd(II) ions, as well as the presence of hydroxyl groups. This fact was proved by XPS results, in which hydroxyl groups and carbon-based groups could have helped in the adsorption process. Besides, the decrease of Na+ ions in aerogels after adsorption, the highest pore density of small pores, and high specific surface area were proved as possible adsorption mechanisms. In the case of Zn(II) adsorption, there was no or minimal adsorption of this ion, showing better adsorption of aerogel to adsorb cadmium ions at pH 4. This higher adsorption for Cd(II) ions is attractive due to the highly toxic character of this ion, which must not exceed the 3.0 ppb limit in contaminated water. The starch aerogel adsorbed between 20 and 30 ppm, a value far above that allowed by legislation, proving the effectiveness of removing Cd(II) ions.

Corroborating the results of cadmium ion adsorption, higher elastic modulus, and mechanical strength, good compression was obtained by the Aero 1:1.5 sample. It showed that smaller pore sizes promote better compressive strength due to lower stress concentration in smaller pores than in larger ones. The application of this material for the adsorption of cadmium ions of highly contaminated sites is due to the presence of hydroxyl groups and high specific surface area, apart from developing dynamic filtration systems to which it mechanically resists, promoting the removal of PTEs from contaminated water.

CRediT authorship contribution statement

All authors contribute to the development and writing of this article and its revision.

Follow below, in Table, recognizing individual author contributions.

Authors	Individual author contributions
Paulo H. Camani	Conceptualization; Methodology; Investigation; Data Curation; Writing - Original Draft Preparation; Visualization; Validation; Formal Analysis; Resources.
Midhun Dominic C.D.	Writing - Original Draft; Investigation; Visualization; Writing - Review & Editing; Validation.
Duclerc F. Parra	Writing - Original Draft; Investigation; Visualization; Validation; Writing - Review & Editing.
Heloísa F. Maltez	Investigation; Methodology; Validation; Data curation; Writing - Original Draft;
Derval S. Rosa	Writing - Review & Editing; Visualization. Conceptualization; Supervision; Resources; Writing - Original Draft; Writing - Review & Editing; Project administration; Funding acquisition.

Declaration of competing interest

The authors declare that they have no known competing financial interests or personal relationships that could have appeared to influence the work reported in this paper.

Data availability

The authors are unable or have chosen not to specify which data has been used.

Acknowledgments

The authors thank the Federal University of ABC (UFABC) and the São Paulo Research Foundation (FAPESP) (2019/16301-6 and 2020/13703-3). The authors also thank the technical support of the Multiuser Experimental Center of UFABC (CEM-UFABC), CECS (UFABC), and REVALORES for assistance. This research used facilities of the Brazilian Nanotechnology National Laboratory (LNNano), part of the Brazilian Centre for Research in Energy and Materials (CNPEM), a private non-profit organization under the supervision of the Brazilian Ministry for Science, Technology, and Innovations (MCTI). The (Scientific Division - Synthesis) staff is acknowledged for the assistance during the experiments (proposal number: 20220371).

References

[1] F. Topuz, T. Holtzl, G. Szekely, Scavenging organic micropollutants from water with nanofibrous hypercrosslinked cyclodextrin membranes derived from green resources, Chem. Eng. J. 419 (2021), https://doi.org/10.1016/j.cej.2021.129443.

[2] M. Lackner, I. Ouattara, G. Na, R. Abolhassani, Clean drinking water global scarcity: a review, J.Water Sci.Eng. 1 (2020) 1–19, https://doi.org/10.5281/zenodo.4084843.

[3] Nadia Morin-Crini, Eric Lichtfouse, Guorui Liu, Vysetti Balaram, Ana Rita Lado Ribeiro, Zhijiang Lu, Friederike Stock, Eric Carmona, Margarida Ribau Teixeira, Lorenzo A. Picos-Corrales, Juan Carlos Moreno-Piraján, Liliana Giraldo, Cui Li, Abhishek Pandey, Didier Hocquet, Giangiacomo Torri, Grégorio Crini, Emerging contaminants: analysis, aquatic compartments and water pollution, in: Emerg Contam, Springer, Cham, 2021, pp. 1–111.

[4] A. Raza, S. Altaf, S. Ali, M. Ikram, G. Li, Recent advances in carbonaceous sustainable nanomaterials for wastewater treatments, Sustain. Mater. Technol. 32 (2022), https://doi.org/10.1016/j.susmat.2022.e00406.

[5] S. Dadari, M. Rahimi, S. Zinadini, Novel antibacterial and antifouling PES nanofiltration membrane incorporated with green synthesized nickel-bentonite nanoparticles for heavy metal ions removal, Chem. Eng. J. 431 (2022), https://doi.org/10.1016/j.cej.2021.134116.

[6] H.G. Hoang, C. Lin, H.T. Tran, C.F. Chiang, X.T. Bui, N.K. Cheruiyot, C.C. Shern, C.W. Lee, Heavy metal contamination trends in surface water and sediments of a river in a highly-industrialized region, Environ. Technol. Innov. 20 (2020), https://doi.org/10.1016/j.eti.2020.101043.

[7] S.F. Ahmed, P.S. Kumar, M.R. Rozbu, A.T. Chowdhury, S. Nuzhat, N. Rafa, T.M. I. Mahlia, H.C. Ong, M. Mofijur, Heavy metal toxicity, sources, and remediation techniques for contaminated water and soil, Environ. Technol. Innov. 25 (2022), 102114, https://doi.org/10.1016/j.eti.2021.102114.

[8] J. Chen, H. Zhang, Q. Wei, U. Farooq, Q. Zhang, T. Lu, X. Wang, W. Chen, Z. Qi, Mobility of water-soluble aerosol organic matters (WSAOMs) and their effects on soil colloid-mediated transport of heavy metal ions in saturated porous media, J. Hazard. Mater. 440 (2022), 129733, https://doi.org/10.1016/j.jhazmat.2022.129733.

[9] M. Zeece, Food additives, in: Introduction to the Chemistry of Food, Elsevier, 2020, pp. 251–311, https://doi.org/10.1016/B978-0-12-809434-1.00007-4.

[10] G. Genchi, M.S. Sinicropi, G. Lauria, A. Carocci, A. Catalano, The effects of cadmium toxicity, Int. J. Environ. Res. Public Health 17 (2020), https://doi.org/10.3390/ijerph17113782.

[11] G. Preet, S. Sidhu, Physiological, biochemical and molecular mechanisms of zinc uptake, toxicity and tolerance in plants, J. Glob. Biosci. 5 (2016) 4603–4633, www.mutagens.co.in.

[12] A. Ali, A.R. Phull, M. Zia, Elemental zinc to zinc nanoparticles: is ZnO NPs crucial for life?Synthesis, toxicological, and environmental concerns, Nanotechnol. Rev. 7 (2018) 413–441, https://doi.org/10.1515/ntrev-2018-0067.

[13] S. Nizamuddin, M.T.H. Siddiqui, N.M. Mubarak, H.A. Baloch, E.C. Abdullah, S. A. Mazari, G.J. Griffin, M.P. Srinivasan, A. Tanksale, Iron oxide nanomaterials for the removal of heavy metals and dyes from wastewater, in: Nanoscale Materials in Water Purification, Elsevier, 2018, pp. 447–472, https://doi.org/10.1016/B978-0-12-813926-4.00023-9.

[14] Gregório Crini, Eric Lichftouse, Green Adsorbents for Pollutant Removal - Fundamentals And Design, Springer, 2018.

[15] X. Liu, Z. Liu, X. Wang, Y. Gao, J. Zhang, T. Fan, X. Ning, S. Ramakrishna, Y.-Z. Long, Superhydrophobic nanofibrous sponge with hierarchically layered structure for efficient harsh environmental oil-water separation, J. Hazard. Mater. 440 (2022), 129790, https://doi.org/10.1016/j.jhazmat.2022.129790.

[16] G. Crini, E. Lichtfouse, L.D. Wilson, N. Morin-Crini, Adsorption-oriented processes using conventional and non-conventional adsorbents for wastewater treatment, in: Green Adsorbents for Pollutant Removal, Springer Nature, Cham, Switzerland, 2018, pp. 23–71, https://doi.org/10.1007/978-3-319-92111-2.

[17] Z. Xu, Q. Zhang, X. Li, X. Huang, A critical review on chemical analysis of heavy metal complexes in water/wastewater and the mechanism of treatment methods, Chem. Eng. J. 429 (2022), https://doi.org/10.1016/j.cej.2021.131688.

[18] S. de Gisi, G. Lofrano, M. Grassi, M. Notarnicola, Characteristics and adsorption capacities of low-cost sorbents for wastewater treatment: a review, Sustain.Mater. Technol. 9 (2016) 10–40, https://doi.org/10.1016/j.susmat.2016.06.002.

[19] R. Wang, L. Deng, X. Fan, K. Li, H. Lu, W. Li, Removal of heavy metal ion cobalt (II) from wastewater via adsorption method using microcrystalline cellulose–magnesium hydroxide, Int. J. Biol. Macromol. 189 (2021) 607–617, https://doi.org/10.1016/j.ijbiomac.2021.08.156.

[20] Pintu Pandit, Kunal Singha, Subhankar Maity, Saptarshi Maiti, Prerana Kane, Treatment of textile wastewater by agricultural waste biomasses, in: Sustainable Technologies for Textile Wastewater Treatments, 2021, pp. 137–156.

[21] P. Kumari, M. Alam, W.A. Siddiqi, Usage of nanoparticles as adsorbents for waste water treatment: an emerging trend, Sustain. Mater. Technol. 22 (2019), https://doi.org/10.1016/j.susmat.2019.e00128.

[22] G. Crini, E. Lichtfouse, L.D. Wilson, N. Morin, Conventional and non-conventional adsorbents for wastewater treatment, Environ. Chem. Lett. 17 (2019) 195–213, https://doi.org/10.1007/s10311-018-0786-8.

[23] N.A. Zubair, E. Abouzari-Lotf, M. Mahmoud Nasef, E.C. Abdullah, Aerogel-based materials for adsorbent applications in material domains, in: E3S Web of Conferences, 2019, pp. 1–12, https://doi.org/10.1051/e3sconf/20199001003.

[24] S. Guo, H. Yuan, F. Liu, W. Luo, B. Li, Y. Yang, H. Jiang, G.J. Cheng, Silver nanowires interlocked graphene aerogel for ultra-high efficient clearage of oil pollution on water, Sustain. Mater. Technol. 29 (2021), https://doi.org/10.1016/j.susmat.2021.e00285.

[25] L. Mo, S. Zhang, F. Qi, A. Huang, Highly stable cellulose nanofiber/polyacrylamide aerogel via in-situ physical/chemical double crosslinking for highly efficient Cu(II) ions removal, Int. J. Biol. Macromol. 209 (2022) 1922–1932, https://doi.org/10.1016/j.ijbiomac.2022.04.167.

[26] B. Geng, Z. Xu, P. Liang, J. Zhang, P. Christie, H. Liu, S. Wu, X. Liu, Three-dimensional macroscopic aminosilylated nanocellulose aerogels as sustainable bio-adsorbents for the effective removal of heavy metal ions, Int. J. Biol. Macromol. 190 (2021) 170–177, https://doi.org/10.1016/j.ijbiomac.2021.08.186.

[27] N. Amaly, A.Y. EL-Moghazy, N. Nitin, G. Sun, P.K. Pandey, Synergistic adsorption-photocatalytic degradation of tetracycline by microcrystalline cellulose composite aerogel dopped with montmorillonite hosted methylene blue, Chem. Eng. J. 430 (2022), https://doi.org/10.1016/j.cej.2021.133077.

[28] A. Muhammad, D. Lee, Y. Shin, J. Park, Recent progress in polysaccharide aerogels: their synthesis, application, and future outlook, Polymers 13 (2021), https://doi.org/10.3390/polym13081347 (Basel).

[29] M.N. Hasan, M.S. Salman, A. Islam, H. Znad, M.M. Hasan, Sustainable composite sensor material for optical cadmium(II) monitoring and capturing from wastewater, Microchem. J. 161 (2021), https://doi.org/10.1016/j.microc.2020.105800.

[30] A. Shahat, K.T. Kubra, M.S. Salman, M.N. Hasan, M.M. Hasan, Novel solid-state sensor material for efficient cadmium(II) detection and capturing from wastewater, Microchem. J. 164 (2021), https://doi.org/10.1016/j.microc.2021.105967.

[31] M.R. Awual, M.M. Hasan, J. Iqbal, M.A. Islam, A. Islam, S. Khandaker, A.M. Asiri, M.M. Rahman, Ligand based sustainable composite material for sensitive nickel (II) capturing in aqueous media, J. Environ. Chem. Eng. 8 (2020), https://doi.org/10.1016/j.jece.2019.103591.

[32] M.R. Awual, A. Islam, M.M. Hasan, M.M. Rahman, A.M. Asiri, M.A. Khaleque, M. Chanmiya Sheikh, Introducing an alternate conjugated material for enhanced lead(II) capturing from wastewater, J. Clean. Prod. 224 (2019) 920–929, https://doi.org/10.1016/j.jclepro.2019.03.241.

[33] M.R. Awual, M.M. Hasan, A.M. Asiri, M.M. Rahman, Cleaning the arsenic(V) contaminated water for safe-guarding the public health using novel composite material, Compos. B Eng. 171 (2019) 294–301, https://doi.org/10.1016/j.compositesb.2019.05.078.

[34] M.R. Awual, M.M. Hasan, A ligand based innovative composite material for selective lead(II) capturing from wastewater, J. Mol. Liq. 294 (2019), https://doi.org/10.1016/j.molliq.2019.111679.

[35] M.N. Arshad, T.A. Sheikh, M.M. Rahman, A.M. Asiri, H.M. Marwani, M.R. Awual, Fabrication of cadmium ionic sensor based on (E)-4-methyl-N′-(1-(pyridin-2-yl) ethylidene)benzenesulfonohydrazide (MPEBSH) by electrochemical approach, J. Organomet. Chem. 827 (2017) 49–55, https://doi.org/10.1016/j.jorganchem.2016.11.009.

[36] M.R. Awual, Ring size dependent crown ether based mesoporous adsorbent for high cesium adsorption from wastewater, Chem. Eng. J. 303 (2016) 539–546, https://doi.org/10.1016/j.cej.2016.06.040.

[37] M.R. Awual, Assessing of lead(III) capturing from contaminated wastewater using ligand doped conjugate adsorbent, Chem. Eng. J. 289 (2016) 65–73, https://doi.org/10.1016/j.cej.2015.12.078.

[38] S.A. El-Safty, M.A. Shenashen, M. Ismael, M. Khairy, M.R. Awual, Optical mesosensors for monitoring and removal of ultra-trace concentration of Zn(ii) and Cu(ii) ions from water, Analyst 137 (2012) 5278–5290, https://doi.org/10.1039/c2an35484e.

[39] M.R. Awual, M.M. Hasan, A. Islam, M.M. Rahman, A.M. Asiri, M.A. Khaleque, M. C. Sheikh, Introducing an amine functionalized novel conjugate material for toxic nitrite detection and adsorption from wastewater, J. Clean. Prod. 228 (2019) 778–785, https://doi.org/10.1016/j.jclepro.2019.04.280.

[40] M.R. Awual, A novel facial composite adsorbent for enhanced copper(II) detection and removal from wastewater, Chem. Eng. J. 266 (2015) 368–375, https://doi.org/10.1016/j.cej.2014.12.094.

[41] M.R. Awual, Novel nanocomposite materials for efficient and selective mercury ions capturing from wastewater, Chem. Eng. J. 307 (2017) 456–465, https://doi.org/10.1016/j.cej.2016.08.108.

[42] M.R. Awual, Solid phase sensitive palladium(II) ions detection and recovery using ligand based efficient conjugate nanomaterials, Chem. Eng. J. 300 (2016) 264–272, https://doi.org/10.1016/j.cej.2016.04.071.

[43] M.R. Awual, A facile composite material for enhanced cadmium(II) ion capturing from wastewater, J. Environ. Chem. Eng. 7 (2019), https://doi.org/10.1016/j.jece.2019.103378.

[44] M.N. Arshad, T.A. Sheikh, M.M. Rahman, A.M. Asiri, H.M. Marwani, M.R. Awual, Fabrication of cadmium ionic sensor based on (E)-4-methyl-N′-(1-(pyridin-2-yl) ethylidene)benzenesulfonohydrazide (MPEBSH) by electrochemical approach, J. Organomet. Chem. 827 (2017) 49–55, https://doi.org/10.1016/j.jorganchem.2016.11.009.

[45] G. Wang, S. Zhang, Q. Zhong, X. Xu, T. Li, Y. Jia, Y. Zhang, W.J.G.M. Peijnenburg, M.G. Vijver, Effect of soil washing with biodegradable chelators on the toxicity of residual metals and soil biological properties, Sci. Total Environ. 625 (2018) 1021–1029, https://doi.org/10.1016/j.scitotenv.2018.01.019.

[46] T. Almubarak, J.H. Ng, R. Ramanathan, H.A. Nasr-El-Din, From initial treatment design to final disposal of chelating agents: a review of corrosion and degradation mechanisms, RSC Adv. 12 (2022) 1813–1833, https://doi.org/10.1039/d1ra07272b.

[47] P.H. Camani, M.G.M. Gonçalo, R.F.S. Barbosa, D. dos S. Rosa, Comprehensive insight of crosslinking agent concentration influence on starch-based aerogels porous structure, J. Appl. Polym. Sci. 138 (2021) 50863, https://doi.org/10.1002/app.50863.

[48] Y. Fang, X. Lv, X. Xu, J. Zhu, P. Liu, L. Guo, C. Yuan, B. Cui, Three-dimensional nanoporous starch-based material for fast and highly efficient removal of heavy metal ions from wastewater, Int. J. Biol. Macromol. 164 (2020) 415–426, https://doi.org/10.1016/j.ijbiomac.2020.07.017.

[49] N. Hammi, S. el Hankari, N. Katir, N. Marcotte, K. Draoui, S. Royer, A. el Kadib, Polysaccharide templated biomimetic growth of hierarchically porous metal-organic frameworks, Microporous Mesoporous Mater. 306 (2020), https://doi.org/10.1016/j.micromeso.2020.110429.

[50] N. Abhari, A. Madadlou, A. Dini, Structure of starch aerogel as affected by crosslinking and feasibility assessment of the aerogel for an anti-fungal volatile release, Food Chem. 221 (2017) 147–152, https://doi.org/10.1016/j.foodchem.2016.10.072.

[51] Z. Wang, W. Zhu, R. Huang, Y. Zhang, C. Jia, H. Zhao, W. Chen, Y. Xue, Fabrication and characterization of cellulose nanofiber aerogels prepared via two different drying techniques, Polymers 12 (2020) 1–13, https://doi.org/10.3390/polym12112583 (Basel).

[52] ASTM International, Standard Test Method for Compressive Properties of Rigid Plastics 1, 2015, https://doi.org/10.1520/D0695-15.

[53] M. Kucharek, W. MacRae, L. Yang, Investigation of the effects of silica aerogel particles on thermal and mechanical properties of epoxy composites, Compos.A: Appl. Sci. Manuf. 139 (2020), https://doi.org/10.1016/j.compositesa.2020.106108.

[54] J.A. Kenar, F.J. Eller, F.C. Felker, M.A. Jackson, G.F. Fanta, Starch aerogel beads obtained from inclusion complexes prepared from high amylose starch and sodium palmitate, Green Chem. 16 (2014) 1921–1930, https://doi.org/10.1039/c3gc41895b.

[55] M. Villegas, A.L. Oliveira, R.C. Bazito, P. Vidinha, Development of an integrated one-pot process for the production and impregnation of starch aerogels in supercritical carbon dioxide, J. Supercrit. Fluids 154 (2019), https://doi.org/10.1016/j.supflu.2019.104592.

[56] I. de Marco, E. Reverchon, Starch aerogel loaded with poorly water-soluble vitamins through supercritical CO2 adsorption, Chem. Eng. Res. Des. 119 (2017) 221–230, https://doi.org/10.1016/j.cherd.2017.01.024.

[57] P. Herman, I. Fábián, J. Kalmár, Mesoporous silica-gelatin aerogels for the selective adsorption of aqueous Hg(II), ACS Appl. Nano Mater. 3 (2020) 195–206, https://doi.org/10.1021/acsanm.9b01903.
[58] J. Li, S. Tan, Z. Xu, Anisotropic nanocellulose aerogel loaded with modified uio-66 as efficient adsorbent for heavy metal ions removal, Nanomaterials 10 (2020) 1–13, https://doi.org/10.3390/nano10061114.
[59] Y. Li, M. Zhou, G.I.N. Waterhouse, J. Sun, W. Shi, S. Ai, Efficient removal of cadmium ions from water by adsorption on a magnetic carbon aerogel, <sb: contribution><sb:title>Environ. Sci. Pollut.</sb:title></sb:contribution><sb: host><sb:issue><sb:series><sb:title>Res.</sb:title></sb:series></sb: issue></sb:host> 28 (2021) 5149–5157, https://doi.org/10.1007/s11356-020-10859-0.
[60] M. Li, S.A. Messele, Y. Boluk, M. Gamal El-Din, Isolated cellulose nanofibers for Cu (II) and Zn (II) removal: performance and mechanisms, Carbohydr. Polym. 221 (2019) 231–241, https://doi.org/10.1016/j.carbpol.2019.05.078.
[61] J. Meng, H. Guan, X. Dai, X. Wang, Amino-functionalized wood aerogel for efficient removal of copper ions from water, Int. J. Polym. Sci. 2021 (2021), https://doi.org/10.1155/2021/4913226.
[62] M.M. Rahman, I. Hafez, M. Tajvidi, A. Amirbahman, Highly efficient iron oxide nanoparticles immobilized on cellulose nanofibril aerogels for arsenic removal from water, Nanomaterials 11 (2021), https://doi.org/10.3390/nano11112818.
[63] N. Sazali, Z. Harun, N. Sazali, A review on batch and column adsorption of various adsorbent towards the removal of heavy metal, J. Adv. Res. Fluid Mech. Therm. Sci. 67 (2020) 66–88, www.akademiabaru.com/arfmts.html, www.akademiabaru.com/arfmts.html.
[64] T.T. Li, Z. Wang, H.T. Ren, H.K. Peng, X. Zhang, Q. Jiang, C.W. Lou, J.H. Lin, Recyclable and degradable nonwoven-based double-network composite hydrogel adsorbent for efficient removal of Pb(II) and Ni(II) from aqueous solution, Sci. Total Environ. 758 (2021), https://doi.org/10.1016/j.scitotenv.2020.143640.
[65] P. Wei, H. Lou, X. Xu, W. Xu, H. Yang, W. Zhang, Y. Zhang, Preparation of PP non-woven fabric with good heavy metal adsorption performance via plasma modification and graft polymerization, Appl. Surf. Sci. 539 (2021), https://doi.org/10.1016/j.apsusc.2020.148195.
[66] O. Omodara, O.O. Daramola, J.L. Olajide, A.A. Adediran, O.S. Akintayo, B. O. Adewuyi, D.A. Desai, E.R. Sadiku, Improved mechanical and wear characteristics of hypereutectic aluminium-silicon alloy matrix composites and empirical modelling of the wear response, Cogent Eng. 7 (2020), https://doi.org/10.1080/23311916.2020.1787010.
[67] R. Albash, C. Yousry, A.M. Al-Mahallawi, A.A. Alaa-Eldin, Utilization of PEGylated cerosomes for effective topical delivery of fenticonazole nitrate: in-vitro characterization, statistical optimization, and in-vivo assessment, Drug Deliv. 28 (2021) 1–9, https://doi.org/10.1080/10717544.2020.1859000.
[68] E.S. Ferreira, C.A. Rezende, Simple preparation of cellulosic lightweight materials from eucalyptus pulp, ACS Sustain. Chem. Eng. 6 (2018) 14365–14373, https://doi.org/10.1021/acssuschemeng.8b03071.
[69] M. Dogenski, P. Gurikov, V. Baudron, J.V. de Oliveira, I. Smirnova, S.R. S. Ferreira, Starch-based aerogels obtained via solvent-induced gelation, Gels 6 (2020) 1–12, https://doi.org/10.3390/gels6030032.
[70] S. Członka, M.F. Bertino, J. Kośny, N. Shukla, Density and shrinkage as guiding criteria for the optimization of the thermal conductivity of poly(urethane)-class aerogels, J. Solgel Sci. Technol. 93 (2020) 149–167, https://doi.org/10.1007/s10971-019-05161-6.
[71] J.P. Vareda, A. Lamy-Mendes, L. Durães, A reconsideration on the definition of the term aerogel based on current drying trends, Microporous Mesoporous Mater. 258 (2018) 211–216, https://doi.org/10.1016/j.micromeso.2017.09.016.
[72] V. Baudron, P. Gurikov, I. Smirnova, S. Whitehouse, Porous starch materials via supercritical-and freeze-drying, Gels 5 (2019) 9–13, https://doi.org/10.3390/gels5010012.
[73] N. Buchtová, C. Pradille, J.L. Bouvard, T. Budtova, Mechanical properties of cellulose aerogels and cryogels, Soft Matter 15 (2019) 7901–7908, https://doi.org/10.1039/c9sm01028a.
[74] K. Ganesan, A. Barowski, L. Ratke, B. Milow, Influence of hierarchical porous structures on the mechanical properties of cellulose aerogels, J. Solgel Sci. Technol. 89 (2019) 156–165, https://doi.org/10.1007/s10971-018-4828-2.
[75] L. Wang, M. Sánchez-Soto, T. Abt, M.L. Maspoch, O.O. Santana, Microwave-crosslinked bio-based starch/clay aerogels, Polym. Int. 65 (2016) 899–904, https://doi.org/10.1002/pi.5104.
[76] K. Wu, Y. Fang, H. Wu, Y. Wan, H. Qian, F. Jiang, S. Chen, Improving konjac glucomannan-based aerogels filtration properties by combining aerogel pieces in series with different pore size distributions, Int. J. Biol. Macromol. 166 (2021) 1499–1507, https://doi.org/10.1016/j.ijbiomac.2020.11.029.
[77] Y.W. Zhao, M.Z. Tian, P. Huang, Starch/clay aerogel reinforced by cellulose nanofibrils for thermal insulation, Cellulose 28 (2021) 3505–3513, https://doi.org/10.1007/s10570-021-03750-9.
[78] R. Wang, Y. Li, X. Shuai, J. Chen, R. Liang, C. Liu, Development of pectin-based aerogels with several excellent properties for the adsorption of Pb2+, Foods 10 (2021) https://doi.org/10.3390/foods10123127.
[79] M. Mu, Y. Li, H.Y. Yu, Z. Li, Y. Cao, X. Chen, Construction of nanocellulose aerogels with mechanical flexibility and pH-responsive properties via a cross-linker structure design strategy, ACS Sustain. Chem. Eng. 9 (2021) 9951–9960, https://doi.org/10.1021/acssuschemeng.1c03503.
[80] K. Ganesan, T. Budtova, L. Ratke, P. Gurikov, V. Baudron, I. Preibisch, P. Niemeyer, I. Smirnova, B. Milow, Review on the production of polysaccharide aerogel particles, Materials 11 (2018) 2144, https://doi.org/10.3390/ma11112144.
[81] M. Thommes, K. Kaneko, A.v. Neimark, J.P. Olivier, F. Rodriguez-Reinoso, J. Rouquerol, K.S.W. Sing, Physisorption of gases, with special reference to the evaluation of surface area and pore size distribution (IUPAC Technical Report), <sb:contribution><sb:title>Pure Appl. </sb:title> </sb:contribution> <sb: host> <sb:issue> <sb:series> <sb:title> Chem.</sb:title></sb:series></sb: issue></sb:host> 87 (2015) 1051–1069, https://doi.org/10.1515/pac-2014-1117.
[82] T.B. da Costa, M.G.C. da Silva, M.G.A. Vieira, Effective recovery of ytterbium through biosorption using crosslinked sericin-alginate beads: a complete continuous packed-bed column study, J. Hazard. Mater. 421 (2022), https://doi.org/10.1016/j.jhazmat.2021.126742.
[83] T. Lei, S.J. Li, F. Jiang, Z.X. Ren, L.L. Wang, X.J. Yang, L.H. Tang, S.X. Wang, Adsorption of cadmium ions from an aqueous solution on a highly stable dopamine-modified magnetic nano-adsorbent, Nanoscale Res. Lett. 14 (2019), https://doi.org/10.1186/s11671-019-3154-0.
[84] B.S. Zadeh, H. Esmaeili, R. Foroutan, Cadmium(II) removal from aqueous solution using microporous eggshell: kinetic and equilibrium studies, <sb: contribution><sb:title>Indones.</sb:title></sb:contribution><sb:host><sb: issue><sb:series><sb:title>J. Chem.</sb:title></sb:series></sb:issue></sb: host> 18 (2018) 265–271, https://doi.org/10.22146/ijc.28789.
[85] N.F. Zon, S. Azman, N.H. Abdullah, N.S. Supian, Kinetics and isotherm of cadmium adsorption onto polyethylene microbeads in artificial seawater, in: IOP Conf Ser Earth Environ Sci, Institute of Physics Publishing, 2020, https://doi.org/10.1088/1755-1315/476/1/012130.
[86] M.R. Awual, M. Khraisheh, N.H. Alharthi, M. Luqman, A. Islam, M. Rezaul Karim, M.M. Rahman, M.A. Khaleque, Efficient detection and adsorption of cadmium(II) ions using innovative nano-composite materials, Chem. Eng. J. 343 (2018) 118–127, https://doi.org/10.1016/j.cej.2018.02.116.
[87] W. Bai, L. Fan, Y. Zhou, Y. Zhang, J. Shi, G. Lv, Y. Wu, Q. Liu, J. Song, Removal of Cd2+ ions from aqueous solution using cassava starch–based superabsorbent polymers, J. Appl. Polym. Sci. 134 (2017), https://doi.org/10.1002/app.44758.
[88] M.T. Bankole, A.S. Abdulkareem, I.A. Mohammed, S.S. Ochigbo, J.O. Tijani, O. K. Abubakre, W.D. Roos, Selected heavy metals removal from electroplating wastewater by purified and polyhydroxylbutyrate functionalized carbon nanotubes adsorbents, Sci. Rep. 9 (2019), https://doi.org/10.1038/s41598-018-37899-4.
[89] M.A. Islam, M.J. Angove, D.W. Morton, B.K. Pramanik, M.R. Awual, A mechanistic approach of chromium (VI) adsorption onto manganese oxides and boehmite, J. Environ. Chem. Eng. 8 (2020), https://doi.org/10.1016/j.jece.2019.103515.
[90] M. Hasanpour, M. Hatami, Application of three dimensional porous aerogels as adsorbent for removal of heavy metal ions from water/wastewater: a review study, Adv. Colloid Interf. Sci. 284 (2020), https://doi.org/10.1016/j.cis.2020.102247.
[91] Mu. Naushad, A.A. Alqadami, A.A. Al-Kahtani, T. Ahamad, Md.R. Awual, T. Tatarchuk, Adsorption of textile dye using para-aminobenzoic acid modified activated carbon: kinetic and equilibrium studies, J. Mol. Liq. 296 (2019), 112075, https://doi.org/10.1016/j.molliq.2019.112075.
[92] W. Liu, Y. Zhang, S. Wang, L. Bai, Y. Deng, J. Tao, Effect of pore size distribution and amination on adsorption capacities of polymeric adsorbents, Molecules 26 (2021), https://doi.org/10.3390/molecules26175267.
[93] G. Zhou, J. Luo, C. Liu, L. Chu, J. Crittenden, Efficient heavy metal removal from industrial melting effluent using fixed-bed process based on porous hydrogel adsorbents, Water Res. 131 (2018) 246–254, https://doi.org/10.1016/j.watres.2017.12.067.
[94] M.M. Rahman, T.A. Sheikh, A.M. Asiri, M.R. Awual, Development of 3-methoxyaniline sensor probe based on thin Ag2O@La2O3 nanosheets for environmental safety, New J. Chem. 43 (2019) 4620–4632, https://doi.org/10.1039/c9nj00415g.
[95] H. Musarurwa, N.T. Tavengwa, Application of carboxymethyl polysaccharides as bio-sorbents for the sequestration of heavy metals in aquatic environments, Carbohydr. Polym. 237 (2020), https://doi.org/10.1016/j.carbpol.2020.116142.
[96] P. Yang, L. Yang, Y. Wang, L. Song, J. Yang, G. Chang, An indole-based aerogel for enhanced removal of heavy metals from water: via the synergistic effects of complexation and cation-π interactions, J. Mater. Chem. A Mater. 7 (2019) 531–539, https://doi.org/10.1039/c8ta07326k.
[97] K.T. Kubra, M.S. Salman, M.N. Hasan, A. Islam, M.M. Hasan, M.R. Awual, Utilizing an alternative composite material for effective copper(II) ion capturing from wastewater, J. Mol. Liq. 336 (2021), https://doi.org/10.1016/j.molliq.2021.116325.
[98] H.Md. Munjur, Md.N. Hasan, Md.R. Awual, Md.M. Islam, M.A. Shenashen, J. Iqbal, Biodegradable natural carbohydrate polymeric sustainable adsorbents for efficient toxic dye removal from wastewater, J. Mol. Liq. 319 (2020), 114356, https://doi.org/10.1016/j.molliq.2020.114356.
[99] A. Wang, S. Li, H. Chen, Y. Hu, X. Peng, Synthesis and characterization of a novel microcrystalline cellulose-based polymeric bio-sorbent and its adsorption performance for Zn(II), Cellulose 26 (2019) 6849–6859, https://doi.org/10.1007/s10570-019-02563-1.
[100] T.S. Anirudhan, L. Divya, C.D. Bringle, P.S. Suchithra, Removal of copper(II) and zinc(II) from aqueous solutions using a lignocellulosic-based polymeric adsorbent containing amidoxime chelating functional groups, Sep. Sci. Technol. 45 (2010) 2383–2393, https://doi.org/10.1080/01496395.2010.490819.
[101] M. Dardouri, F. Ammari, A. BelHadj Amor, F. Meganem, Adsorption of cadmium (II), zinc (II) and iron (III) from water by new cross-linked reusable polystyrene adsorbents, Mater. Chem. Phys. 216 (2018) 435–445, https://doi.org/10.1016/j.matchemphys.2018.06.002.

[102] X. Pei, L. Gan, Z. Tong, H. Gao, S. Meng, W. Zhang, P. Wang, Y. Chen, Robust cellulose-based composite adsorption membrane for heavy metal removal, J. Hazard. Mater. 406 (2020), 124746.
[103] Y. Ma, L. Cheng, D. Zhang, F. Zhang, S. Zhou, Y. Ma, J. Guo, Y. Zhang, B. Xing, Stabilization of Pb, Cd, and Zn in soil by modified-zeolite: mechanisms and evaluation of effectiveness, Sci. Total Environ. 814 (2022), https://doi.org/10.1016/j.scitotenv.2021.152746.
[104] F. Wang, Y. Zhu, A. Wang, Preparation of carboxymethyl cellulose-based macroporous adsorbent by eco-friendly Pickering-MIPEs template for fast removal of Pb2+ and Cd2+, Front. Chem. 7 (2019) 1–15.
[105] X. Xie, X. Zhao, X. Luo, T. Su, Y. Zhang, Z. Qin, H. Ji, Mechanically activated starch magnetic microspheres for Cd(II) adsorption from aqueous solution, Chin. J. Chem. Eng. 33 (2021) 40–49, https://doi.org/10.1016/j.cjche.2020.06.003.
[106] R.S. Vieira, M.L.M. Oliveira, E. Guibal, E. Rodríguez-Castellón, M.M. Beppu, Copper, mercury and chromium adsorption on natural and crosslinked chitosan films: an XPS investigation of mechanism, Colloids Surf. A Physicochem. Eng. Asp. 374 (2011) 108–114, https://doi.org/10.1016/j.colsurfa.2010.11.022.
[107] H. Faghihian, H. Nourmoradi, M. Shokouhi, Performance of silica aerogels modified with amino functional groups in PB(II) and CD(II) removal from aqueous solutions, <sb:contribution><sb:title>Pol. J.</sb:title></sb:contribution><sb:host><sb:issue><sb:series><sb:title>Chem. Technol.</sb:title></sb:series></sb:issue></sb:host> 14 (2012) 50–56, https://doi.org/10.2478/v10026-012-0059-4.
[108] X. Hao, S. Yang, T. E, Y. Li, High efficiency and selective removal of Cu(II) via regulating the pore size of graphene oxide/montmorillonite composite aerogel, J. Hazard. Mater. 424 (2022), https://doi.org/10.1016/j.jhazmat.2021.127680.
[109] M.R. Awual, M.M. Hasan, A. Islam, A.M. Asiri, M.M. Rahman, Optimization of an innovative composited material for effective monitoring and removal of cobalt(II) from wastewater, J. Mol. Liq. 298 (2020), https://doi.org/10.1016/j.molliq.2019.112035.